THE SENSITIVITY OF THERMALLY DRIVEN MOUNTAIN FLOWS TO LAND COVER CHANGE

by

Justin A. W. Cox

A dissertation submitted to the faculty of
The University of Utah
in partial fulfillment of the requirements for the degree of

Doctor of Philosophy

Department of Meteorology

The University of Utah

December 2005

ABSTRACT

The influence of heterogeneous land cover on the boundary layer and surface conditions was examined in the mountainous, semi-arid Wasatch Front region of northern Utah. In addition, sensitivity studies were conducted to evaluate the effect of land cover change on surface temperatures and on the depth of the convective boundary layer. Using the Pennsylvania State University/National Center for Atmospheric Research fifth-generation Mesoscale Model, the Great Salt Lake and Utah Lake were found to play a dominant role in modulating the depth of the convective boundary layer, while areas of urban and agricultural land cover exerted local effects. Subsidence arising from slope flows and a cross-valley circulation were not found to have a large impact on the boundary layer in this case.

In order to simulate the conditions that existed prior to large-scale human habitation, a simulation was conducted in which all anthropogenic land cover types (e.g., urban, residential, agricultural) in the initial simulation, termed the 1992 run, were changed to grassland. This was termed 1847 run. Compared to the 1847 run, the convective boundary layer in the 1992 run was deeper over urban land and shallower over irrigated cropland. In addition, the lake breeze front was faster to arrive in the urbanized area of the Salt Lake Valley, but slower to move past. This was a result of the convergent circulation over the locally warm urban area. It is hypothesized that as urban land increasingly replaces agricultural land in semi-arid regions, local temperature and convective boundary layer depth anomalies, as well as non-local effects on the lake breeze, will have more dramatic effects than the urbanization of natural land cover.

CHAPTER 1

INTRODUCTION AND LITERATURE REVIEW

Humans have been altering the landscape of the earth and composition of the atmosphere for millennia. Within the past 200 years, it has become increasingly evident that the earth system is sensitive to such changes. In addition to increases to greenhouse gas concentrations resulting from thousands of years of anthropogenic deforestation and irrigation (Ruddiman 2003), the industrial revolution and population explosion of the past two centuries have spawned rampant urbanization and fossil fuel combustion. Globally, the proportion of the population living in cities has increased from 29% in 1950 to 47% in 2000, and is projected to increase to 61% by 2030 (United Nations 2004). The area of urban land has increased to accommodate the additional inhabitants, resulting in changes to the characteristics of the earth's surface. The effects of urbanization on climate and weather have been well documented (e.g., Howard 1833; Bornstein 1968; Oke 1982).

Weather and climate changes associated with urbanization have important implications for city residents. Urbanization is often associated with surface temperature anomalies such as the urban heat island (UHI) and the oasis effect, which have important implications for energy use and human comfort (Sailor 1995). In addition, increased emissions of pollutants in cities and changes to the boundary layer structure can exacerbate or mitigate air quality problems.

Changes in local and regional atmospheric processes associated with urbanization are complex and difficult to generalize (Oke 1982), but we now have the computational and observational tools to explore how particular urbanization scenarios affect meteorology and climate. Neither a theoretical nor a purely observational study, this dissertation attempts to bridge the gap between generalized theoretical studies and specific case studies. A modeling approach is used to determine the sensitivity of local thermally driven winds and boundary layer structure to land cover change.

This next chapter provides a brief literature review on the relevant meteorological features of this dissertation: namely, thermally driven flows generated by land surface heterogeneities and slope and valley flows. Chapter 2 examines numerical simulations of anomalous boundary layer development in the urbanized Salt Lake Valley, and the factors leading to the phenomenon. Chapter 3 builds on this case analysis with a series of sensitivity studies in which boundary layer development is compared for various land cover scenarios. Conclusions are drawn in Chapter 4, along with recommendations for future work.

1.1 Thermally driven mesoscale circulations

The focus of this dissertation is upon boundary layer processes and thermally direct circulations on a diurnal time scale. The sea breeze is probably the best known thermally driven circulation, noted in the scientific literature as early as the 17th century by Halley (Rotunno 1983), but also documented by the ancient Greeks (Neumann 1973).

Daytime heating results in higher temperatures over a land surface than over water, owing to the greater heat capacity of water. Over land, the resulting low pressure at the surface and high pressure aloft yields a vertical circulation that is compensated by onshore

flow at the surface, and offshore return flow aloft. Similarly, greater nighttime cooling over land induces an offshore land breeze, with onshore return flow aloft. Landmark papers addressing the mathematical analysis of sea and land breezes are reviewed by Rotunno (1983).

In addition to sea breezes, other circulations with similar causes have been documented (e.g., Segal and Arritt 1992). Following their convention, these will be referred to as "nonclassical mesoscale circulations" (NCMCs). As with sea breezes, NCMCs can be generated by differential sensible heat fluxes produced by spatial gradients in heat capacity. Other thermal properties, such as available water for evaporation and soil conductivity, and radiative properties such as shortwave albedo and longwave emissivity, can also produce horizontal contrasts in sensible heat flux to the atmosphere. For example, albedo, thermal conductivity, and latent heat flux differences between salt flats and surrounding desert regions are responsible for playa breezes (Rife et al. 2002). Similarly, horizontal differences in these parameters due to snow cover or vegetation can drive local winds (e.g., Segal et al. 1991, Segal et al. 1989). Lastly, aerodynamic contrasts can lead to enhanced or suppressed mechanical mixing and therefore affect vertical and horizontal momentum transport (Grimmond and Oke 1999).

Anthropogenic land cover change often results in landscape contrasts that lead to NCMCs, and can yield broader meteorological consequences (e.g., Marshall et al. 2004; Pielke et al. 1999; Chase et al. 1999). Marshall et al. (2004) simulated a three-month summer period in Florida for several land cover situations, focusing on the change from natural wetlands to drained agricultural land. The increased sensible heat flux arising from this

land cover transformation resulted in the enhancement of the lake breeze front, a decrease in convective precipitation, and increased maximum daytime surface temperatures.

Urbanization often leads to differential heating relative to surrounding non-urban areas. The urban heat island (UHI) is commonly defined as a positive temperature anomaly compared to surrounding areas. A UHI can drive its own circulation, known as a heat island circulation (HIC). The characteristics of a UHI, its HIC, and the mechanisms responsible for them depend on urban and rural characteristics, and on the local climate regime. The UHI phenomenon was first noted in the scientific literature by Howard (1833), and since then it has garnered attention as an obvious signal of man's impact on the environment.

Meteorological measurements are normally taken near the earth's surface. In a city, we can define the urban canopy layer (UCL) as the atmosphere below the tops of buildings. The heat island as measured in the UCL has different characteristics than the UHI measured in the urban boundary layer (UBL), which extends above roof level (Oke 1995). The UBL UHI is more important for questions of boundary layer structure, turbulent transport, and pollutant concentration. For these reasons, this study will focus on the characteristics of the boundary layer as a whole.

Bornstein (1968) presented observations of the UHI in New York City, measured by helicopter throughout the UBL. Increases in ground heat storage in the urban fabric, anthropogenic heat fluxes, reduced surface moisture, and atmospheric pollution were cited as possible causes of the temperature anomaly. The urban area cooled off more slowly than the surrounding countryside, resulting in weaker and less-frequent nocturnal inversions. This behavior is typical; UHIs are often strongest at night (e.g., Bornstein 1968;

Oke 1982; Draxler 1986; Morris et al. 2001). Elevated inversion layers were observed over the urban area, while lower atmospheric layers were less stably stratified. Atkinson (2003) ran sensitivity studies using a numerical model of an idealized urban area configured to resemble London, England. Among the various possible contributors (albedo, anthropogenic heat, emissivity, roughness length, sky view factor, surface resistance to evaporation, and thermal inertia), surface resistance to evaporation was the most important factor controlling heat island strength during the day, while anthropogenic heating dominated at night. The increased roughness length associated with urbanization was the only factor to decrease the strength of the heat island, by increasing turbulent mixing in the surface layer.

The treatment of these surface processes in numerical models has evolved from simplistic to complex, and care must be taken to ensure that the surface characteristics are properly specified. Current state of the art land surface parameterizations include sophisticated treatments of heat and moisture fluxes through multiple soil and snow layers; radiative transfer and heat and moisture fluxes through plant canopies; and modified drag terms for areas with large roughness elements such as forests or cities (e.g., Walko et al. 2000, Lakhtakia and Warner 1994; Sellers et al. 1986). The benefits of such elaborate parameterizations are still being evaluated. Zhong and Fast (2003) found that some of these schemes yielded less accurate surface temperatures than a simpler scheme, perhaps because the model has been tuned for the simpler scheme and would require some adjustment to reap the full benefits of the more complex parameterization. In addition, these complicated parameterizations are especially sensitive to the specification of surface characteristics.

Intercomparison and validation of land surface schemes remains an ongoing challenge (Henderson-Sellers et al. 1995).

In conclusion, the basic mechanisms of sea breezes and NCMCs are well understood. In real situations, the driving forces behind these circulations can interact in complicated ways, making accurate simulations difficult. In addition, the variety of surface characteristics that can affect these winds makes each situation unique, with characteristics varying in space and time.

1.2 Slope and valley flows

Slope and valley flows are similar in some ways to the flows discussed in the previous section, but some fundamental differences are discussed here. For the purposes of this discussion, the following terminology will be used. Slope flows refer to winds that blow directly up or down the local gradient of a slope. Upslope flows (common during daytime) are also known as anabatic winds. Downslope flows (common at night) are also known as katabatic or drainage winds. Valley flows blow along a valley axis, and are often perpendicular to slope flows. The term “topographic flows” will refer to any or all of these winds as a group.

The flux of sensible heat to or from a slope results in a horizontal temperature gradient between the air just over the slope and the air at the same level away from the slope. This gives rise to ascent along a heated slope, and descent along a cooled slope. Poulos (1996) provides an excellent review of the literature on katabatic flows, the highlights of which are mentioned here. Analytical models of slope flows have explained these winds using various dynamic and thermodynamic forcing terms; Mahrt (1982) defined several types of

downslope flows in terms of the relevant forcing mechanisms, based on a scale analysis of the momentum equations.

Compared to downslope flows, there has been very little attention given to upslope flows. Since the theoretical treatments of Prandtl (1952) and Defant (1949), there have been few papers regarding the understanding of daytime upslope winds. They occur under generally benign conditions, and are considered relevant mainly because of their role in heat transport within the valley atmosphere, though valley venting can occur as a result of converging upslope flows on ridge tops (e.g., De Wekker 2002; Reuten et al. 2005).

Heat transport by upslope and downslope winds often gives rise to larger-scale topographic flows. For example, converging down-slope flows result in rising motion and adiabatic cooling over the valley center. The air in the valley center is then colder than the air over the adjacent plain. McNider and Pielke (1984) summarized the mechanisms that drive nocturnal slope and valley flows with an idealized valley-plain model. Down-valley flow occurs in the valley atmosphere (i.e., up to the height of the surrounding mountains), even for a non-sloping valley floor. The reverse occurs as a result of upslope flow during the day (Rampanelli et al. 2004), with slope flows transporting heat from the valley sidewalls into the middle of the valley through a cross-valley circulation and compensating subsidence, a mechanism first proposed by Whiteman (1982) in his discussion of the breakup of nocturnal temperature inversions in valleys.

Whiteman (1990) presented detailed observations of slope, valley, and basin flows. These observations generally confirmed the theoretical understanding of valley flows, but also highlighted some of the complexities that occur in real situations. For example, the following factors can cause deviations from classical slope/valley flow patterns: along-

valley changes in topography, differential heating of slopes with different aspects and slope angles, ridgetop geometry, and variations in surface energy properties.

Several studies of local-scale thermally driven flows have been conducted in arid places such as the Intermountain West. Hawkes (1947) provided a detailed review of the mechanisms driving mountain and valley winds in northern Utah, and still stands as a benchmark reference for the history of topographic flow research. Zeller (1972) partitioned the components of the total wind in the PBL in the Salt Lake Valley according to theoretically determined mountain-valley, land-lake, barrier, and urban effects. Stewart et al. (2002) demonstrated the importance of thermally driven flows in the Intermountain West and described the diurnal cycles of slope and valley wind systems in the Salt Lake region. Their climatology encompassed the combined effects of the mountain/plain, valley, slope, land/lake, and urban wind systems, under the condition of weak synoptic forcing. It demonstrated clearly the clockwise and counterclockwise turning of winds on right and left valley sidewalls caused by the interaction between slope and valley flows, and the variability in transition times between daytime and nighttime flow regimes. Rife et al. (2002) described a playa breeze in Utah's West Desert and performed sensitivity studies to determine the effects of the Great Salt Lake and topography on thermally driven flows there. The Great Salt Lake, the salt playas, and the local topography each play a role in shaping the diurnal evolution of winds and boundary layer structure. Stone and Hoard (1990) documented the daytime mountain/valley wind in the valleys of northern Utah, focusing on the Tooele and Rush valleys from January to August, covering winter and summer regimes. They reported that for their period of study, daytime upvalley flows

occurred on about 50% of the days, confirming the importance of regional mountain winds to the local climate.

Mesoscale models have been shown to simulate topographic flows adequately, although some errors in timing, magnitude, and character do exist (e.g., de Wekker 2002; Zhong and Fast 2003; Weigel 2005). These errors can largely be attributed to the treatment of the atmospheric boundary layer and land surface processes in the models. Topographic flows are phenomena that exist and are generated in the lowest several hundred meters of the atmosphere, a region where complicated turbulent exchange processes are traditionally represented statistically, with the result that potentially important microscale features are not resolved. Improvements to boundary layer representations are likely to be expensive and complicated, and their costs may or may not be justified by improvements to the resulting simulations. Simulations of slope flows in mesoscale models are constrained by the vertical grid spacing of the models and by computational power.

Topographic flows continue to be the subject of much research and debate in the field of mountain meteorology research, especially as high-resolution simulations become less expensive and the effects of topographic flows on boundary layer evolution are better understood.

1.3 Land surface/slope flow interactions

In the real world, local surface winds are driven by a combination of forcing mechanisms. A simple example is the reinforcement of a sea breeze by topographic flows from inland mountains (e.g., Mahrer and Pielke 1977). Lake and topography influences in Peru reinforce one another in generating thermally direct circulations (Stivari et al. 2003). Rife

et al. (2002) described the interactions between synoptic forcing, lake, playa, and topographic flows in northern Utah. Each played an important part in the complex evolution of the boundary layer of the area. Pielke et al. (1993) found that mesoscale albedo differences in northern Arizona had an effect on surface sensible heat flux that was sufficient to compete with the local topographic flows there.

The studies of Hertig (1995) and Kitada et al. (1998) demonstrated the importance of urban areas in modifying topographic flows in Switzerland and Japan, respectively. Urbanization in small Swiss cities affects the mixing depth and magnitude of topographic flows (Hertig 1995), but this study found surface roughness changes to be the cause, rather than urban temperature effects. Kitada et al. (1998) stated that, although topographic flows were the single most important factor in determining surface winds on the Nohbi Plain, the city of Nagoya, located on the Nohbi Plain, acted against the sea breeze to form a weak wind convergence zone inland of the city. The sea breeze was generated by an offshore pressure gradient that, on the inland side of Nagoya, was opposed by a pressure gradient generated by Nagoya's UHI. Ohashi and Kida (2002) simulated the effects of Osaka and Kyoto, Japan, on the local sea breeze circulation. Using idealized simulations, they determined that the interaction of urban and land/sea breezes can produce a modified flow regime, called a "chain flow", that extends far inland. Under this scenario, pollutants emitted from a coastal city would be transported to an inland city more effectively than by either the sea breeze or urban breeze alone. On the other hand, Schultz and Warner (1982) found that in Los Angeles, the urban area did not have a significant impact on the stronger sea breeze and topographic flows there.

The magnitude of the urbanization impact on climate is sensitive to both the local climate regime and to the nature of the land cover change. It remains a major research challenge to determine how, in various situations, urbanization interacts with other local forcing factors to alter local wind systems. Because generalizing the effects of urbanization on local weather is impossible, the problem must be broken down into more specific pieces. For example, how do the convective boundary layer and topographic flows evolve in a mountainous, arid climate like that of Salt Lake City? And, how have they been affected by urban land cover change in the form of increased irrigation and the widespread use of impervious building materials? These questions will be addressed in chapters 2 and 3, respectively.

CHAPTER 2

PROCESSES CONTRIBUTING TO ANOMALOUS CBL EVOLUTION IN A MOUNTAINOUS SEMI-ARID VALLEY

2.1 Introduction

The evolution of the planetary boundary layer (PBL) under anticyclonic conditions has important consequences for urban meteorology and air quality. During the day, a convective boundary layer (CBL) typically develops, and over flat homogeneous terrain, increases in depth as a result of turbulent sensible heat flux convergence, until the surface layer stabilizes because of radiative cooling. Heat, momentum, and pollutants are usually well-mixed through the CBL, and surface pollutant concentrations depend on the height above ground level (AGL) of the CBL top (henceforth referred to as the CBL depth, see de Wekker 2002). Contrasts in heat and momentum fluxes arising from land surface heterogeneities can produce local and regional variability in CBL depth and mixing.

In regions of complex terrain and heterogeneous land cover, deviations from this model of CBL evolution often occur. In mountain valleys, for example, CBL depths may decrease after the time of maximum heating, rather than increase until sunset (Kuwagata and Kimura, 1995, 1997; and Weigel 2005). The modeling study of Rampanelli et al. (2004) demonstrated such CBL evolution in an idealized valley. Anomalous CBL evolu-

tion can also occur in areas with land surface and sensible heating contrasts. Doran et al. (1995) observed a deep CBL over irrigated farmland in eastern Oregon, an unexpected result because of the low surface sensible heat flux. They hypothesized that the deeper CBL from nearby dry steppes was advected over the irrigated farmland by synoptic and regional-scale winds. In the Salt Lake Valley (SLV) of northern Utah, Shaw and Hubbe (2002) observed decreasing CBL depths in the afternoon.

The climate and terrain of the Intermountain West make the SLV a unique laboratory for studying CBL development in complex terrain. The SLV is bounded on three sides by steep mountains, and to the northwest by the Great Salt Lake (GSL; see Fig. 2.1 for location map). The SLV is 40 km long and 25 km wide with a valley bottom elevation of ~1280 m MSL. Its sidewalls rise to as high as 3000 m MSL over 15 km. Its semi-arid climate distinguishes it from most locations where valley winds have been studied. The average annual precipitation at SLC is <40 cm.

Within and adjacent to the SLV, 1 million people live in Salt Lake City and other cities along the Wasatch Front, creating a significant impact on the natural land cover. Irrigated agriculture and urban and residential land cover much of the SLV and Utah Valley (UV, Fig. 2.1b). A variety of forcing mechanisms produce locally driven winds, including topography, the GSL, and heterogeneous land cover (Doran et al. 2002; Rife et al. 2002). In the SLV, it is difficult to determine the relative contributions of each of these various mechanisms to the resultant wind. The contributions of the GSL, the surrounding terrain, and land cover heterogeneities are considered in aggregate.

Predicting the evolution of the CBL a mountainous, semi-arid climate is an important problem because of rapid urban growth in these areas. Anticyclonic conditions are com-

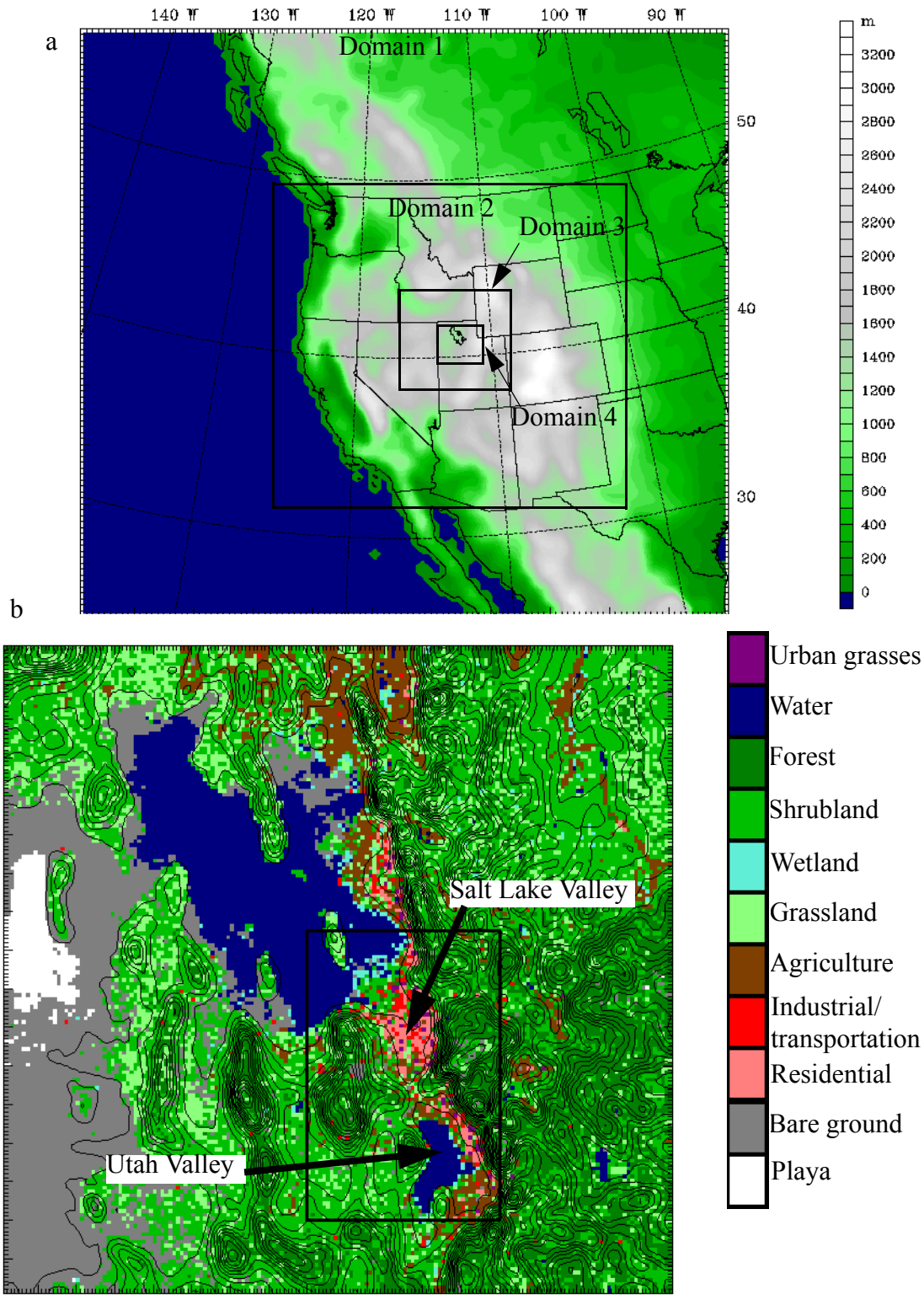

Fig. 2.1. MM5 model domains, showing (a) topography for Domain 1 and locations of nested grids; (b) land cover and topography for Domain 4, with the Salt Lake and Utah valleys bounded by the box.

mon in semi-arid regions. Though these conditions are benign from a weather perspective, air quality is an issue when synoptic forcing is weak and surface processes are decoupled from the free atmosphere. The objective of this study is to describe and diagnose, using a numerical model, the evolution of the daytime CBL depth in the SLV under anticyclonic conditions. The results of this study will have broad implications for understanding CBL evolution over mountain valleys, particularly those adjacent to bodies of water, such as along mountainous coastlines.

The following section summarizes the model setup and experimental domain of this study. A case overview and brief model validation are provided in section 2.3. Section 2.4 presents the model results, which are discussed in section 2.5. The final section presents conclusions and recommendations for future work.

2.2 Model setup and observations

This study examines 16 October 2000, the day preceding Intensive Observing Period 6 (IOP6) of the Vertical Transport and Mixing Experiment (VTMX), hereafter referred to as "the study period". VTMX was a field campaign designed to improve understanding of the processes leading to the vertical mixing of heat, momentum, and air pollutants in the stable boundary layer in complex terrain (Doran et al. 2002). This date was chosen because it was synoptically quiescent, clear, and offered the availability of special VTMX observations collected for model validation.

Because VTMX examined the stable nocturnal boundary layer and morning and evening transitions, the available daytime observations are substantial, but not as comprehensive as those collected at night. Radiosonde observations were collected from the Salt

Lake City International Airport (SLC), Wheeler Farm, and Jordan Narrows (NCAR) at various intervals (see Table 2.1 and Fig. 2.2 for times and station locations), and high-density surface observations from the MesoWest cooperative networks (see Horel et al. 2002).

Table 1: Important sites and observation times

Name	Abbreviation	Times LST on 16 October 2000
Salt Lake City	SLC	0400, 1000, 1600
Wheeler Farm	Wheeler	1500, 1600
Jordan Narrows	NCAR	1700

The Pennsylvania State University (PSU)/National Center for Atmospheric Research (NCAR) fifth generation Mesoscale Model (MM5) version 3.7 was used to simulate the study period. The MM5 is a nonhydrostatic finite difference model that uses a terrain-following sigma vertical coordinate (Grell et al. 1995). Four one-way nested domains with grid spacings of 36, 12, 4, and 1.33 km were used, the innermost covering northern Utah and centered over the SLV (Figure 2.1). In the vertical, 51 variably spaced full-sigma levels were used, corresponding to spacings of 7-9 hPa near the surface and 37.5 hPa near the model top (100 hPa)[1]. Physics options are listed in Table 2.2. Cloud and precipitation pro-

Table 2: MM5 Physics Options

Radiation	Boundary layer	Surface fluxes	Microphysics	Convection
Cloud radiation scheme (Dudhia 1989)	MRF (Troen and Mahrt 1986; Hong and Pan 1996)	5-layer ground heat budget model	Reisner2	Kain-Fritsch2, domains 1 and 2 (Kain 2004)

1. The full sigma levels were at σ=1.00, 0.99, 0.98, 0.97, 0.96, 0.95, 0.94, 0.93, 0.92, 0.91, 0.90, 0.89, 0.88, 0.87, 0.86, 0.85, 0.84, 0.83, 0.82, 0.81, 0.80, 0.79, 0.78, 0.77, 0.76, 0.75, 0.74, 0.73, 0.72, 0.71, 0.69, 0.67, 0.65, 0.62, 0.59, 0.56, 0.53, 0.50, 0.47, 0.44, 0.41, 0.37, 0.33, 0.29, 0.25, 0.21, 0.17, 0.13, 0.09, 0.05, and 0.00

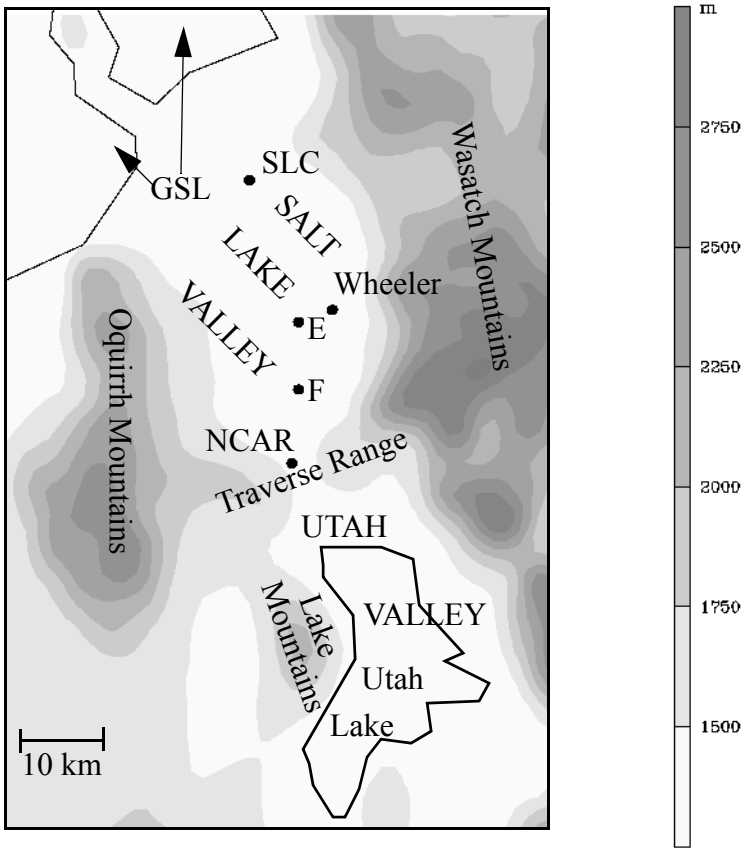

Fig. 2.2. Topography and important locations in the SLV. SLC is the Salt Lake City International Airport; Wheeler is Wheeler Farm radiosonde site; NCAR is the Jordan Narrows radiosonde site; E and F are valley-bottom analysis locations.

cesses were not important since clear skies prevailed. The MRF PBL parameterization (see Troen and Mahrt 1986, and Hong and Pan 1996) uses four different regimes for turbulent diffusivity parameters, (1) stable, (2) damped mechanically driven turbulence, (3) forced convection, and (4) free convection. The regime is determined by the bulk Richardson number and the ratio h/L, where h is the boundary layer depth and L is the Monin-Obukhov length scale. The stability parameters for heat and momentum (essentially corrections to K-theory calculations to account for non-local turbulent fluxes) depend on the surface roughness, the height of the lowest σ-level, and the Monin-Obukhov length. For the majority of the study period, the free convection regime dominated.

A simple 5-layer ground heat budget model (hereafter 5-layer model) was used instead of a complex coupled land surface model (LSM) for several reasons. First, despite its simplicity, Zhong and Fast (2003) found that the 5-layer model produced more accurate simulations in the Salt Lake Valley than did the LSM. Second, its simplicity allows for a more intuitive analysis of the surface representation, and a more direct specification of land-cover characteristics. Finally, the 5-layer model is more easily initialized, unlike complex LSMs which ideally require a spin-up period.

Model land cover was defined using the United States Geological Survey (USGS) National Land Cover Data (NLCD) 1992 database (Vogelmann et al. 2001; see Fig. 2.1). This database has two advantages over those accessed by the default MM5 software. First, it includes more urban land cover types. Second, it better replicates the patchy distribution of urban land areas over the SLV. The scale of land cover patches is an important factor in

mesoscale circulations (Zhong and Doran 1995; Baidya Roy et al. 2003). Table 2.3 pre-

Table 3: Land cover characteristics

Land cover	Moisture availability (fraction)	Heat capacity (MJ m^{-3} K^{-1})	Roughness length (m)	Albedo (fraction)	Thermal inertia (J m^{-2} K^{-1} $s^{-1/2}$)
Grassland	0.15	2.08	0.1	0.23	1675
Shrubland	0.10	2.08	0.1	0.25	1675
Cropland	0.50	2.50	0.05	0.23	1675
Forest	0.60	2.92	0.5	0.12	2094
Wetland	0.75	2.92	0.2	0.14	2513
Open water	1.00	-NA-	10^{-4}	0.08	2513
Playa	0.40	1.20	0.01	0.40	2094
Bare ground	0.05	1.20	0.1	0.25	837
Residential	0.10	1.89	0.91	0.15	1256
Commercial/ industrial	0.10	1.89	1.08	0.15	1256

sents the characteristics of the most prevalent land cover types. It is important to note that considerable urban growth has occurred along the Wasatch Front even since 1992, so even this updated land cover database underestimates the urban land cover.

The most significant differences between the urban and non-urban (primarily grass-land, shrubland, and agricultural land) land cover in the valleys were in moisture availabil-ity and roughness length. Moisture availability was specified according to land cover type and was independent of time, a reasonable approximation because of the short runtime of the model and the lack of precipitation during the study period. Lake surface temperatures were explicitly specified and held fixed at 287 K, the average temperature of the GSL in October (Steenburgh et al. 2000) and near the median value observed during VTMX

(Doran et al. 2002). Again, this was an acceptable assumption based on the short model runtime.

The largest potential source of uncertainty in these model runs is in the specification of surface characteristics. Default MM5 surface characteristics were used for all land cover types, with two exceptions. First, roughness lengths were specified for each urban category following Burian et al. (2002). Second, moisture availability values for grassland and shrubland were decreased relative to the default values to more closely simulate the semi-arid conditions of the region. Surface energy budget observations in the Intermountain West were used to validate the choice of moisture availability (Malek and Bingham 1997; Ivans 2005). Moisture availability is an especially important parameter that can vary greatly under typical weather conditions. October weather is typically quite variable, with average temperatures at SLC ranging from 17.0 °C at the beginning of the month to 9.4 °C at the end, with extremes of 35.6 and -10 °C. In addition, total October precipitation has ranged from 0.0 to 99.3 mm water equivalent. This makes the specification of representative surface characteristics very difficult. For this case, it was assumed that the moisture availability was relatively low, representing a period with little precipitation and plants that are in senescence (transpiring little water to the atmosphere).

For model initialization, the gridded analysis from the National Centers for Environmental Prediction (NCEP) Eta model (Black 1994; Rogers et al. 1995, 1996) was interpolated from its native grid (80 km horizontal grid spacing; 50 hPa vertical grid spacing) onto each domain's horizontal grid at 1700 LST 15 October 2000. Thereafter, Eta model analyses for lateral boundary conditions were generated at 12-h intervals until 0500 LST 17 October 2000.

Points E and F (see Fig. 2.2) were chosen for detailed analyses because of their locations in the valley bottom, away from the valley sidewalls and because of the contrast in land cover between the two sites. The locations of these sites allow valley and lake breezes to be examined with minimal influence from slope flows, as suggested by Segal et al. (1997). In addition, E is located on the western edge of a large contiguous urban area, while F is located in a primarily agricultural region. This allows for the local effects of different land cover types to be examined.

2.3 Case overview and model performance

Clear skies and light crest-level (700 hPa) winds prevailed during the study period, allowing thermally driven winds to develop. Fig 2.3 shows the NCEP Eta model analysis at 0500 LST (1200 UTC) 16 October 2000. At 500 hPa, the geopotential height gradient indicates large-scale zonal flow over the western United States with a weak short-wave ridge moving eastward into Utah behind an exiting short-wave trough. At crest level (700 hPa), relative humidities are low (<60%) and winds are light (<5 m s^{-1}) and northwesterly with little or no temperature advection.

Simulated and observed potential temperature profiles are shown in Fig. 2.4. The observed sounding prior to sunrise (0400 LST) shows a shallow nocturnal inversion (Fig. 2.4a). A weakly stable atmosphere extends to ~3 km AGL where it is capped by a stronger stable layer. The simulated surface temperature is ~5 K too warm and the nocturnal inversion is weaker than observed, as is often seen in mesoscale model simulations under similar conditions (e.g., Hanna and Yang 2001; Zhong and Fast 2003; Hart et al. 2004). The profile above the surface is better simulated, though the model fails to reproduce the fine

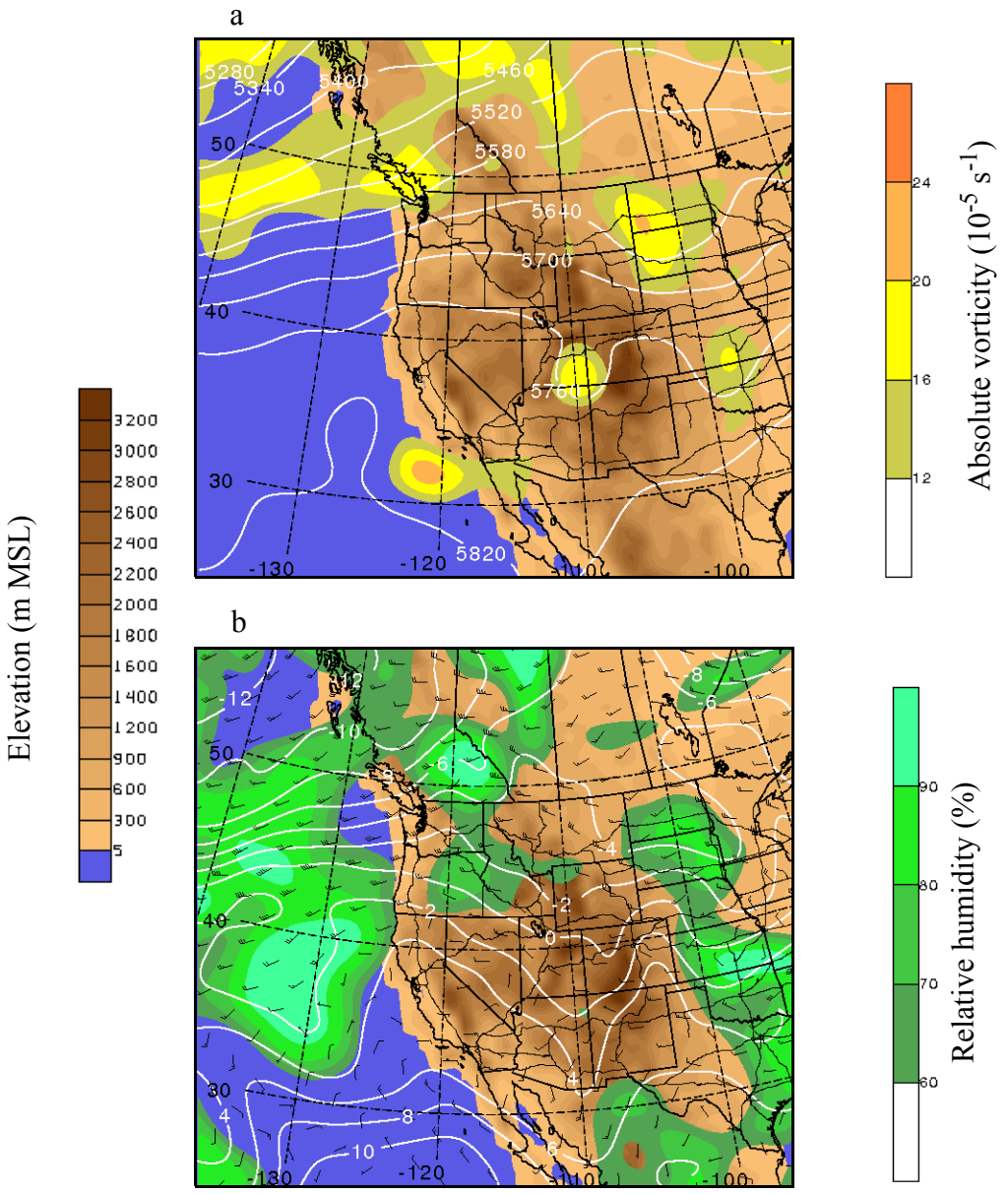

Fig. 2.3. Eta model analyses at 0500 LST (1200 UTC) 16 October 2000. (a) 500 hPa heights (m MSL) and absolute vorticity; (b) 700 hPa isotherms (°C), winds, and relative humidity. Full and half barbs indicate 5 and 2.5 m s^{-1}, respectively. Terrain shading colorbar at left; colorbars for individual plots at right.

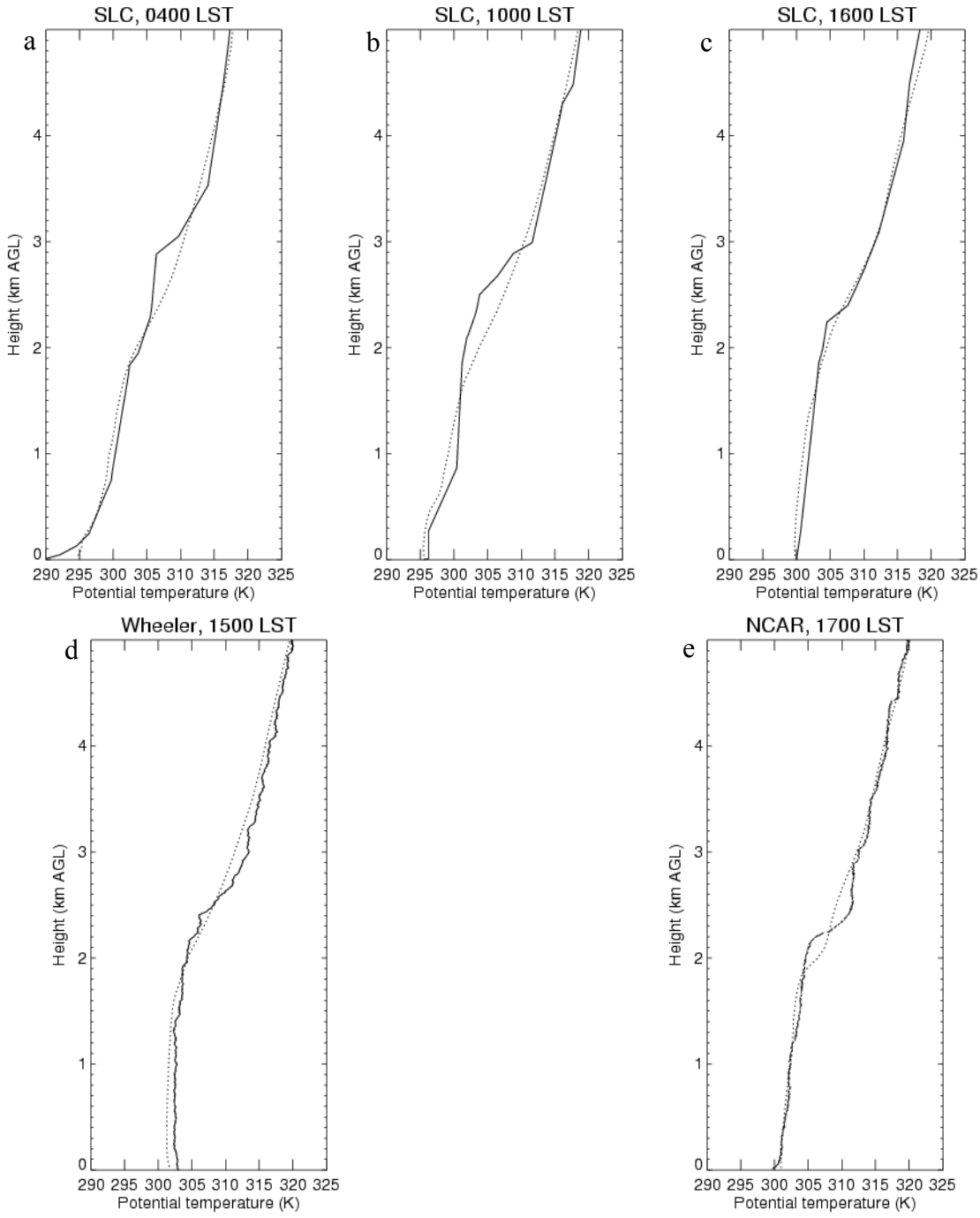

Fig. 2.4. Potential temperature profiles on 16 October 2000. (a) SLC at 0400; (b) SLC at 1000; (c) SLC at 1600; (d) Wheeler at 1500; (e) NCAR at 1700. Solid lines are observed soundings; dotted lines are MM5 soundings for the same locations.

scale structure near the capping stable layer. By mid-morning (1000 LST), a shallow mixed layer develops near the surface, and a series of stable and well-mixed layers exists between 0.5 and 3 km AGL (Fig. 2.4b). The shallow mixed layer is reproduced by the simulation but is 0.1 km too deep. The simulation fails to reproduce the complex multi-layered structure, but the model error is never more than 3 K at any elevation. In the mid-afternoon (1600 LST), there is a weakly stable layer extending from the surface to ~2.3 km AGL, capped by a sharp transition to a very stable layer (Fig. 2.4c). The MM5 reproduces the weakly stable layer well, but does not capture the sharpness of the transition at the top of the weakly stable layer. The 1500 LST sounding at Wheeler (Fig. 2.4e) is well-mixed from the surface to ~2.1 km AGL, above which the atmosphere becomes more stable. The MM5 simulates the observed sounding well, though it is 1 K too cold at the surface and fails to capture the sharpness of the transition to the stable layer at the top of the mixed layer at 2.4 km AGL. The late afternoon (1700 LST) boundary layer at NCAR (Fig. 2.4d) is similar to that at SLC, weakly stable from the surface up to a capping stable layer at ~2.1 km AGL. The simulated sounding at NCAR reproduces the capping stable layer well, but places it 0.1 km too low.

Fig. 2.5 shows a time series of simulated and observed surface winds (10 m simulated winds, interpolated from the lowest 1/2-σ level using similarity theory) at SLC. The observed wind shifts from downvalley (southerly component) to upvalley (northerly component) between 1300 and 1400 LST, while the MM5 transition is about an hour later. Figure 2.6 compares the simulated and observed winds at 1400 LST, just after the upvalley wind transition at SLC. The model captures the observed southeasterly flow in the southwestern SLV and upslope westerly flow in the eastern SLV. Differences between modeled

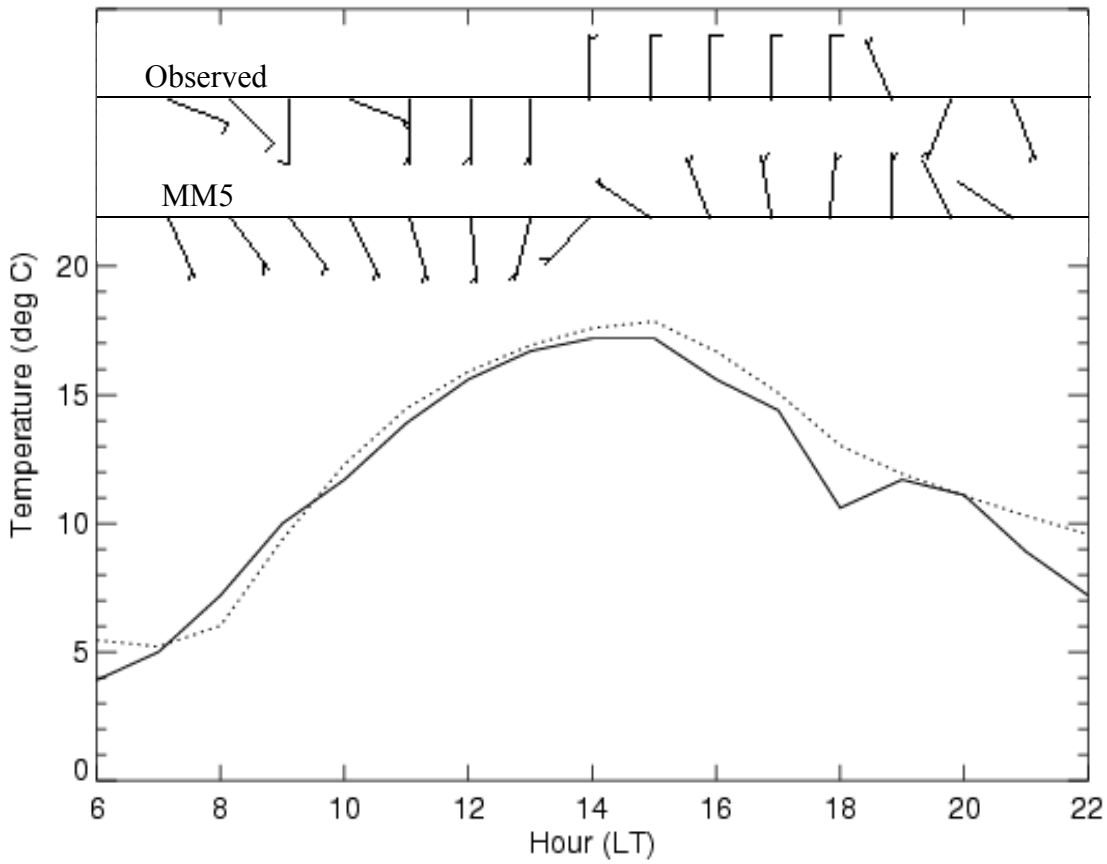

Fig. 2.5. Time series of surface (10 m) winds and (2 m) temperatures on 16 October 2000. Top row of wind barbs is observations from SLC; bottom row is MM5 output for SLC. Full and half barbs denote 5 and 2.5 m s^{-1}, respectively. Solid (dotted) line is observed (MM5) temperature.

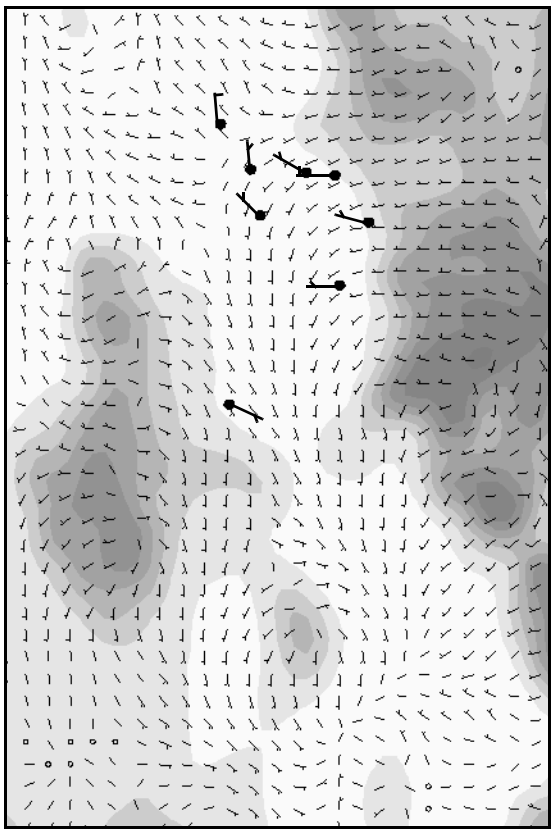

Fig. 2.6. Simulated and observed (in bold) surface winds in the SLV at 1400 LST. Topography shading as in Fig. 2.1.

and observed winds in the northern valley are a result of the delayed transition to upvalley flow immediately behind the simulated LBF. Although the upvalley transition times in the simulation occur later than observed, they fall within an acceptable range when compared to summer-month thermally driven flows in the SLV observed by Stewart et al. (2002), and lake breeze fronts observed by Zumpfe (2004).

In summary, the MM5 produces a physically realistic and plausible simulation for the study period. The temperature and wind fields produced by the MM5 resemble those observed by surface stations and radiosondes in the SLV, although there are some errors in the timing of the LBF. Differences between the observed and simulated vertical profiles of potential temperature can largely be attributed to the limited vertical resolution of the MM5 and acknowledged limitations in the simulation of the PBL.

2.4 Results

2.4.1 Wind, temperature, and CBL features

Figure 2.7a shows surface temperatures and winds at 1100 LST, during the morning transition period, when upslope flows have developed on the sidewalls of the SLV. The surface temperatures are highest in the eastern portion of the SLV, the area with the largest contiguous urban area (see Fig. 2.1b). Along the valley bottom, 3-5 m s^{-1} downvalley flow persists. Cold air advection in the northern Utah Valley and southern SLV extends from the surface to 500 m AGL (Fig. 2.7b). The valley air is generally sinking, and the boundary layer in the central portion of the valley is better-mixed than to the north or south.

By 1300 LST, the CBL has deepened and developed interesting features, so the analysis will focus on CBL depth from here on. The central, mostly urban portion of the SLV

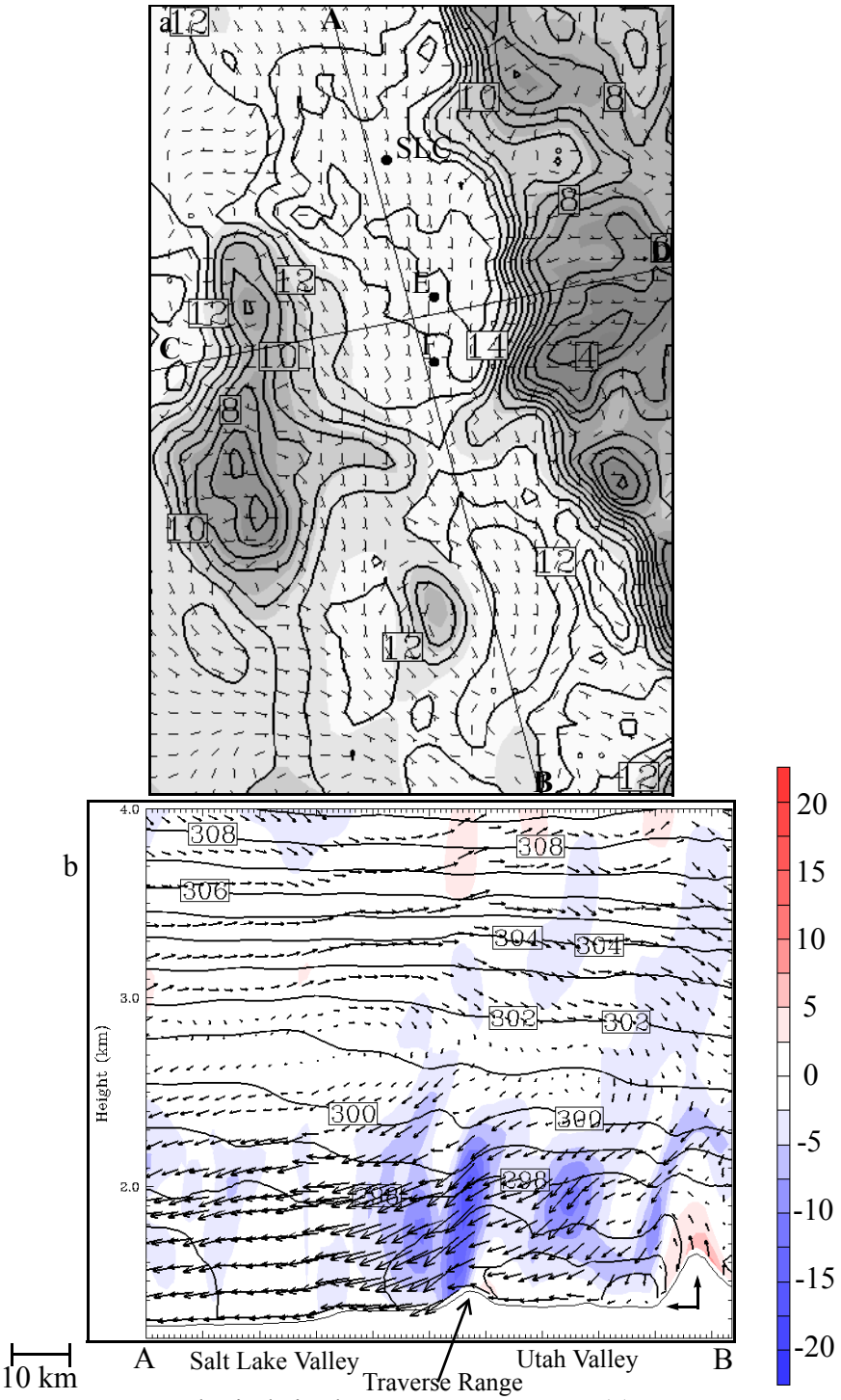

Fig. 2.7. Temperature and winds in the SLV at 1100 LST. (a) 2 m temperatures (°C) and 10 m winds, barbs as in Fig. 2.5, plotted every other grid point; (b) cross section along A-B of potential temperature (contours every 1 K), vertical velocity in colorshading, and circulation vectors. Colorbar indicates vertical velocity in cm s^{-1}. Reference vectors in lower right indicate 5 m s^{-1} horizontal and 15 cm s^{-1} vertical.

shows relatively uniform CBL depths of around 1500 m, 300 m deeper than the CBL at the south end of the valley (Fig. 2.8a). In addition, the northwest corner of the SLV near the shore of the GSL has CBL depths less than 1200 m. The boundaries of the GSL and Utah Lake are clearly evident as strong gradients in CBL depth, as CBL depths over the lake surfaces are <300 m. Surface winds are less than 5 m s^{-1} throughout the SLV, having decreased in strength since 1100 LST.

Figure 2.8b shows a cross section along line A-B (see Fig. 2.8a for location). The LBF, located at the northern end of the cross section A-B, has features that are characteristic of sea breeze fronts (e.g., Reible et al. 1993; Simpson 1994). The position of the LBF is easily identified by a transition from down-valley to up-valley flow, and is coincident with the leading edge of an updraft of >2.5 cm s^{-1} and an increase in water vapor mixing ratio from <4 to >4 g kg^{-1} (not shown).

At the south end of the valley, weak subsidence is occurring in the valley atmosphere below 2.5 km MSL (Fig. 2.8b). A small region of strong subsidence results from southerly flow over the Traverse Range between the UV and SLV, while larger scale, weaker subsidence extends through the valley atmosphere to the LBF. Also evident in Fig. 2.8b is a dome of warm surface air in the middle of the SLV, associated with the commercial/industrial grid cells in that region. The northwest end of the SLV features a concentrated region of rising air at and just in front of the LBF, and colder surface temperatures and sinking air behind the LBF. In cross section C-D (Fig. 2.8c), the cross-valley circulation arising from upslope winds on the valley sidewalls interacts with the westerly component of the synoptic-scale midlevel winds. In addition, subsidence over the valley core is evident. It is not clear that this mid-valley subsidence is a direct result of the cross-valley circulation, as

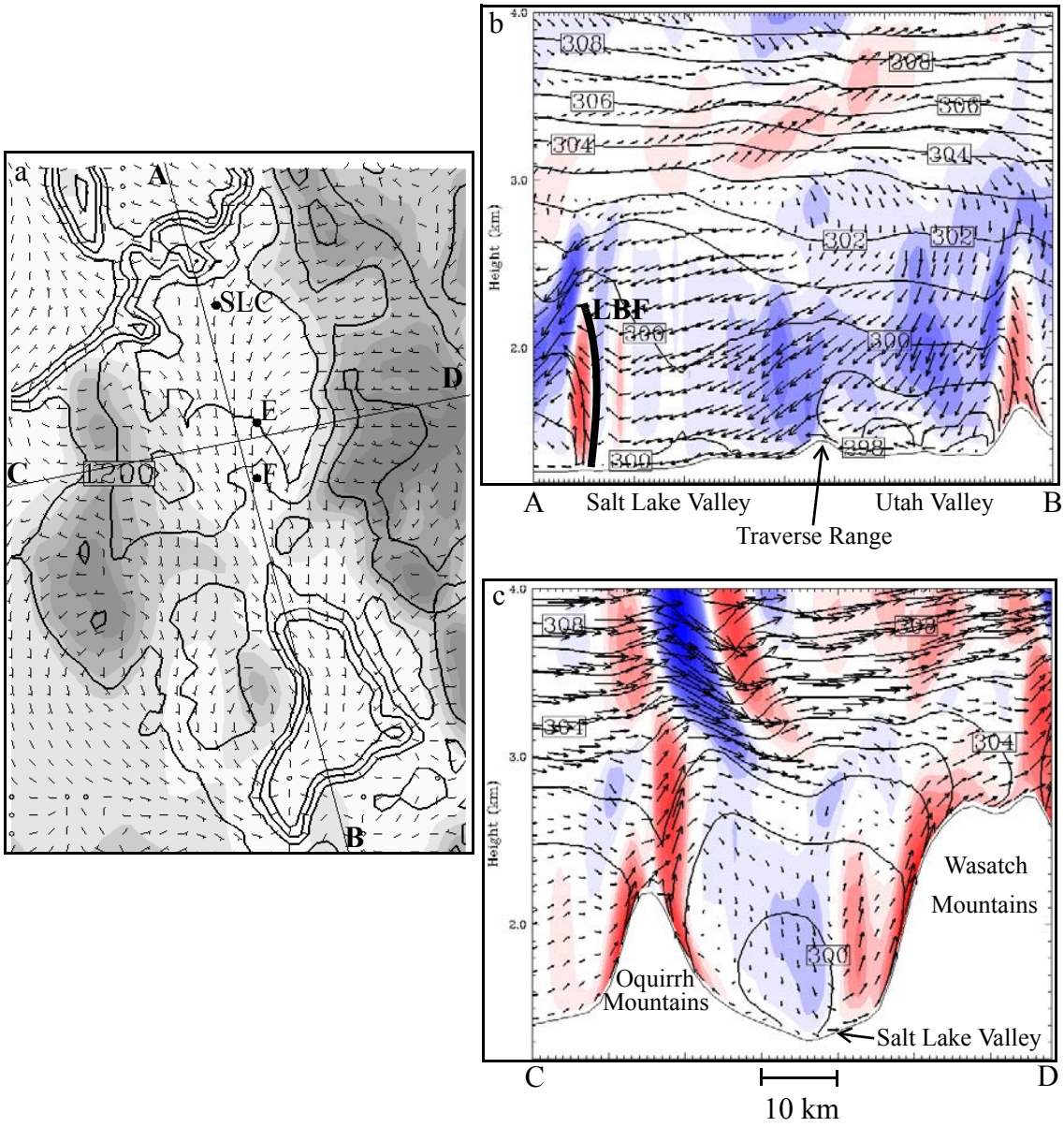

Fig. 2.8. SLV CBL features at 1300 LST. (a) Map view of CBL depths (m AGL); (b) cross section along A-B, showing contours of potential temperature and circulation vectors, vertical velocities in color shading; (c) same as (b) but along C-D.

there is no evidence of mass divergence at the surface along the valley axis, as would be expected.

Two hours later, at 1500 LST (Fig. 2.9a), the CBL in the middle of the SLV has grown to a maximum depth of ~1800 m. The LBF has advanced southeastward, while the region of suppressed CBL depth in the southern SLV persists. The CBL depth in most of the SLV has increased by ~300 m, but the same spatial differences remain. In the southern SLV, the CBL depth is 600 m lower than in the central SLV. CBL depths are deepest where the LBF induces strong rising motion. CBL depths behind the LBF are dramatically lower (Fig. 2.9b) because of the horizontal advection of cool, stable boundary layer air from over the GSL. The along-valley winds are of comparable magnitude (~2.5 m s^{-1}) on both sides of the LBF. The cross-valley circulation has grown stronger since 1300 LST (Fig. 2.9c), with more intense subsidence in the center of the valley and stronger upslope flows on the valley sidewalls. The LBF has maintained the structure of a sea breeze front.

By 1700 LST (Fig. 2.10), the lake breeze front has progressed southward to the middle of the SLV. The LBF has contributed to decreased CBL depths where it has passed. In addition, the decrease in surface heating before sunset results in stabilization of the near-surface atmosphere and a rapid decline in CBL depth. Only on west-facing slopes, which continue to receive sunshine, do CBL depths remain above 300 m. The vertical structure of the LBF has not changed appreciably since 1500 LST (Fig. 2.10b), though mixed layer depths in front of the LBF have decreased by about one third. The strong ascent visible in the cross section C-D is associated with the leading edge of the LBF on the western side of the SLV (Fig. 2.10c).

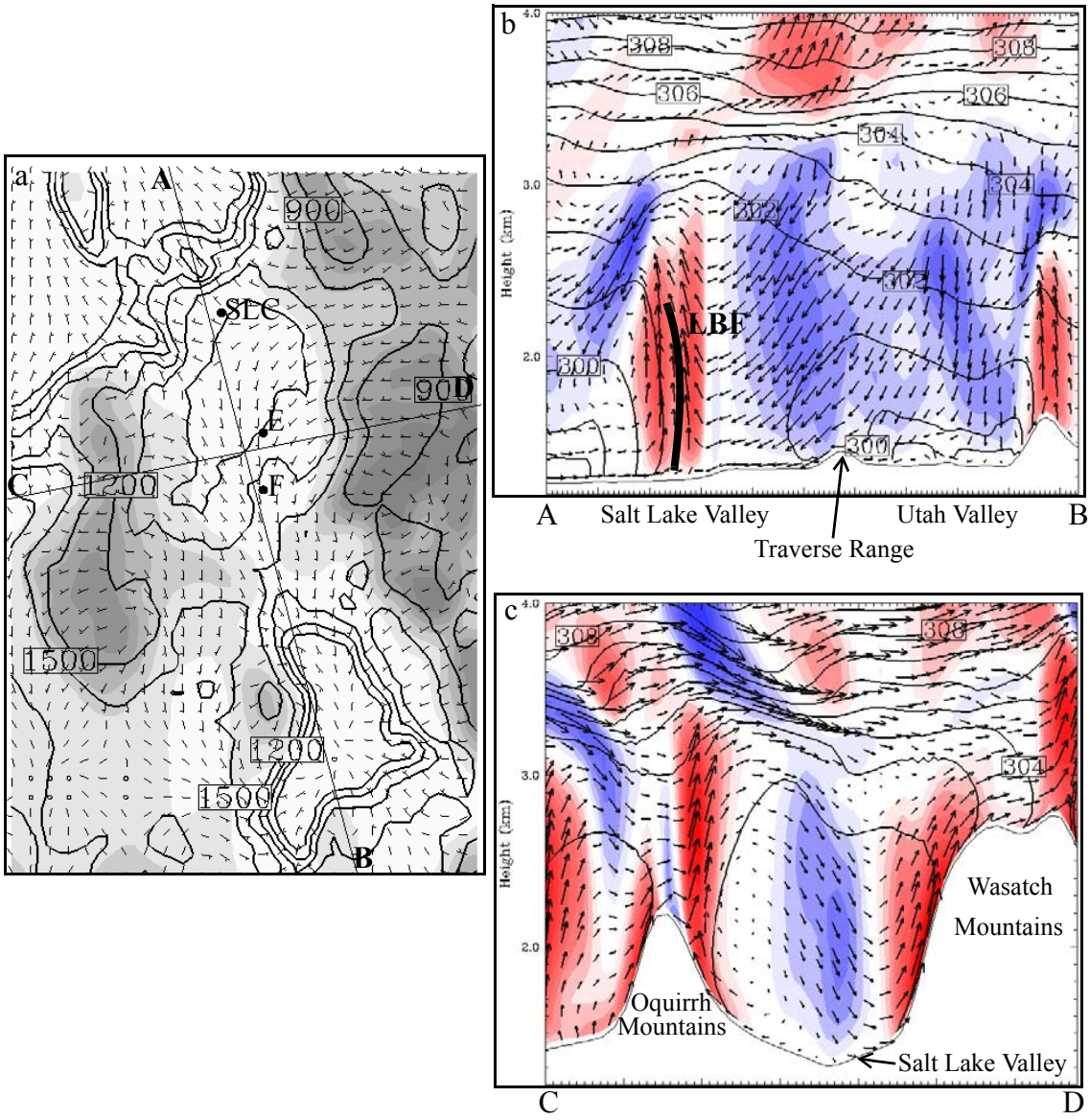

Fig. 2.9. Same as Fig. 2.8 except at 1500 LST.

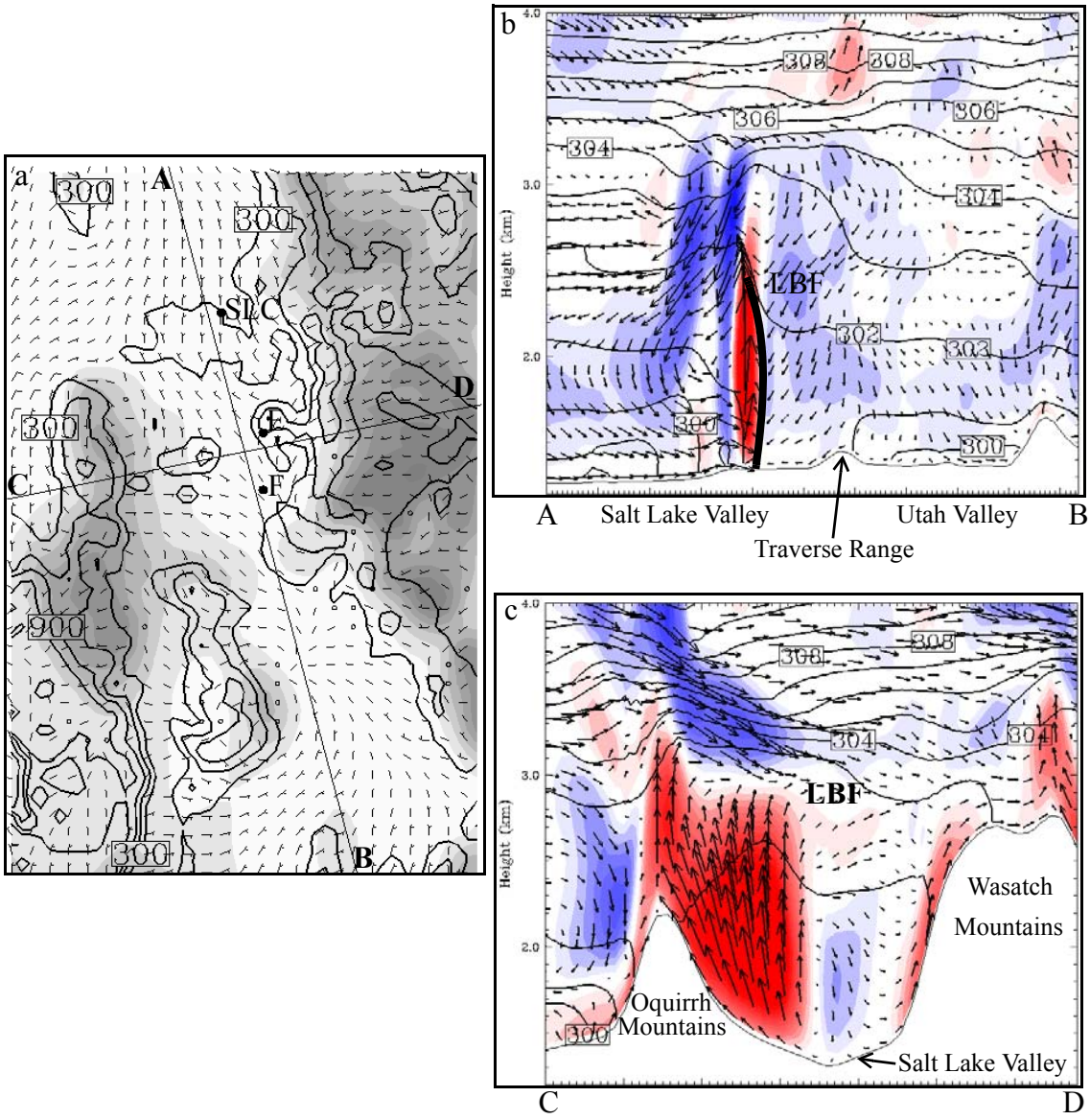

Fig. 2.10. Same as Fig. 2.8 except at 1700 LST.

Time series at SLC, E, and F further illustrate the evolution of CBL depth and wind in the SLV (Fig. 2.11). At SLC, the maximum CBL depth occurs at 1500 LST, around the time of LBF passage (Fig. 2.11a). Between 1500 and 1600 LST, the CBL depth decreases abruptly, while the wind continues veering from southerly to northerly (Fig. 2.11b). At E and F, the time of maximum CBL depth is also 1500 LST, followed by a decline that represents the demise of the CBL as surface radiative cooling begins to dominate the energy balance (Fig. 2.11a). The PBL collapses to a minimum value of 69 m AGL, the height of the lowest full σ level, and hence the lowest level of the surface layer top. Abrupt wind shifts occur after the more gradual decrease in CBL depth (Fig. 2.11b). The LBF does not initiate the decrease in CBL depth at those locations; rather, the CBL becomes shallow before the LBF moves rapidly through the central SLV. The maximum CBL depth at F is ~500 m less than at E or SLC. Two factors are responsible for this discrepancy: greater moisture availability of the agricultural land surrounding F, which leads to lower values of surface sensible heat flux; and cold air advection from the adjacent UV. The patterns of CBL evolution at E and F resemble closely those presented by Troen and Mahrt (1986) for a flat-terrain case (see their Fig. 5). At SLC, on the other hand, the CBL depth is affected by the passage of the LBF, a non-local influence. No evidence for an afternoon decline in valley CBL depth resulting from subsidence in a cross-valley circulation was found, differentiating these results from those of Rampanelli et al. (2004) and Weigel (2005).

Isochrones of the LBF position are presented in Fig. 2.12 as identified by the following criteria: an updraft of >2.5 m s^{-1}, a wind shift from southerly to northerly, and a mixing ratio increase of >1 g kg^{-1}. The lake breeze front moves slowly through the northwest portion of the SLV in the early afternoon, and then advances rapidly southward after 1600

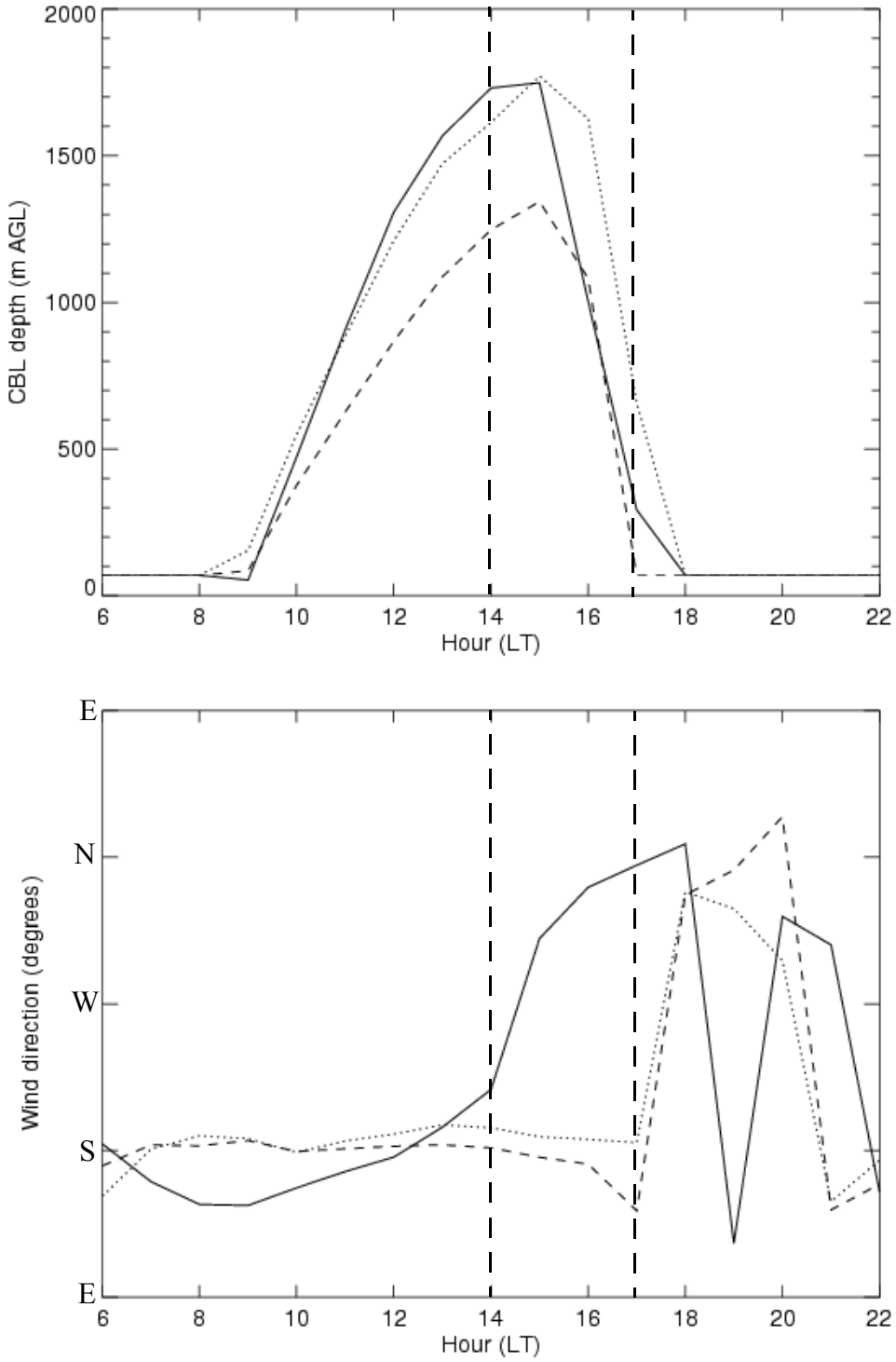

Fig. 2.11. Time series of (a) CBL depth and (b) wind direction. SLC is solid line; E is dotted line; F is dashed line. Vertical dashed lines indicate beginning of upvalley flow transition for SLC (1400 LST) and E and F (1700 LST).

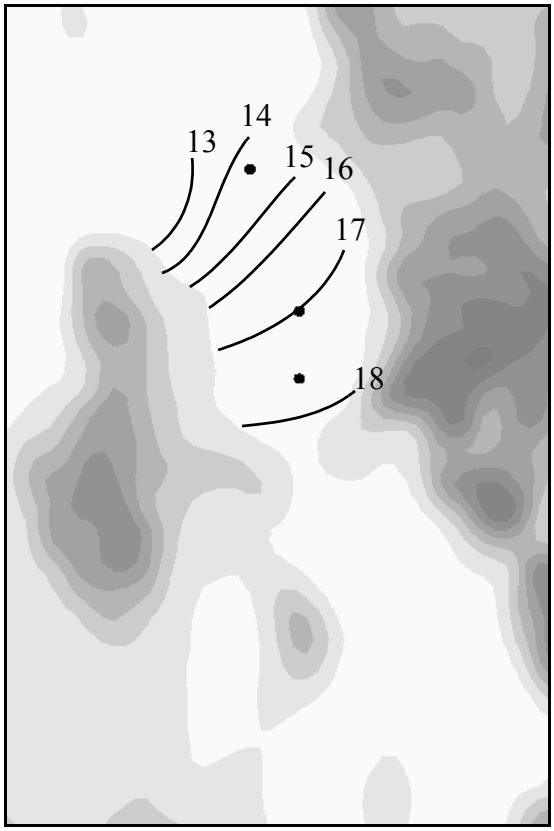

Fig. 2.12. Isochrones of the lake breeze front from 1200 to 1800 LST. SLC, E, and F are denoted by the bullets, but labels have been omitted for clarity. Topography shading as in Fig. 2.1.

LST. This progression is consistent with the characteristics of well-developed sea breeze fronts described by Reible et al. (1993) and Simpson (1994).

2.4.2 Thermodynamic energy budget - temperature tendency terms

The CBL depth is a value that integrates, both spatially and temporally, the characteristics and evolution of local meteorology. A careful analysis of the terms of the thermodynamic energy equation allows for the separation and diagnosis of the contributions of local surface heating and remote (advective) effects. In the MM5, the thermodynamic energy equation has six terms and can be represented by the potential temperature tendency.

$$\frac{\partial \theta}{\partial t} = -(V_h \cdot \nabla \theta) - \left(w \frac{\partial \theta}{\partial z}\right) - \frac{\partial}{\partial z}\overline{w'\theta'} + D_\theta - R$$

I II III IV V VI

Term I is the total instantaneous potential temperature change at a given location. Term II is the horizontal potential temperature advection; term III is the vertical potential temperature advection; term IV is turbulent heat flux divergence; term V is numerical diffusion; and term VI is radiative heat flux divergence.

Since the MM5 horizontal and vertical advection terms are calculated in σ coordinates, the Cartesian horizontal and vertical advection components are estimated in the following way. First, the vertical advection component of the potential temperature tendency is calculated from model variables using a centered-difference method. The horizontal advection term is calculated as a residual of the total advection term (obtained directly from the model output) minus the calculated vertical advection term. This method avoids the pitfalls of interpolation from sloping σ surfaces to a horizontal grid. The turbulent flux divergence and radiative flux divergence terms are obtained directly from the MM5. Radiative flux divergence is small compared to the other terms, and is not presented here.

In general, warming aloft by the vertical advection term indicates a lowering of the CBL top by subsidence. The CBL depth can also be decreased through horizontal cold air advection. During the day, turbulent heat flux convergence generated by surface heating and shear-driven turbulence typically acts to distribute heat from the surface upwards and to deepen the CBL.

Vertical profiles of the components of the thermodynamic energy budget at SLC, E, and F are plotted in Fig. 2.13. At 1200 LST, the total potential temperature tendency is positive and fairly uniform below 3 km AGL at all three locations, except for a diversion to a minimum value at or slightly below the CBL top at each location (Fig. 2.13a,b,c). Turbulent heat flux convergence produces most of the heating at low levels. At E and F, near-surface turbulent heat flux divergence opposes horizontal cold air advection from Utah Lake, which constitutes a source of cold air for the southern SLV during the day. At SLC, on the other hand, horizontal advection from the warm urban core acts together with the turbulent heat flux divergence term to warm the atmosphere. At F, CBL depths are always lower than at SLC or E. Vertical advection of warm air through subsidence at ~1 km AGL acts to suppress the CBL depth at F, despite higher values of turbulent heat flux near the surface (Fig. 2.13c).

By 1600 LST, the LBF has passed SLC (see Fig. 2.12). The potential temperature tendency at the surface has become negative, owing in large part to strong cold air advection in the lowest 0.3 km. This is countered, but not fully balanced, by turbulent heat flux convergence (Fig. 2.13d). The CBL depth is lower now than it was at 1200 LST. At the other locations, on the other hand, the CBL depth has increased but the rate of warming at all elevations has decreased. The passage of the LBF is responsible for the decrease in CBL

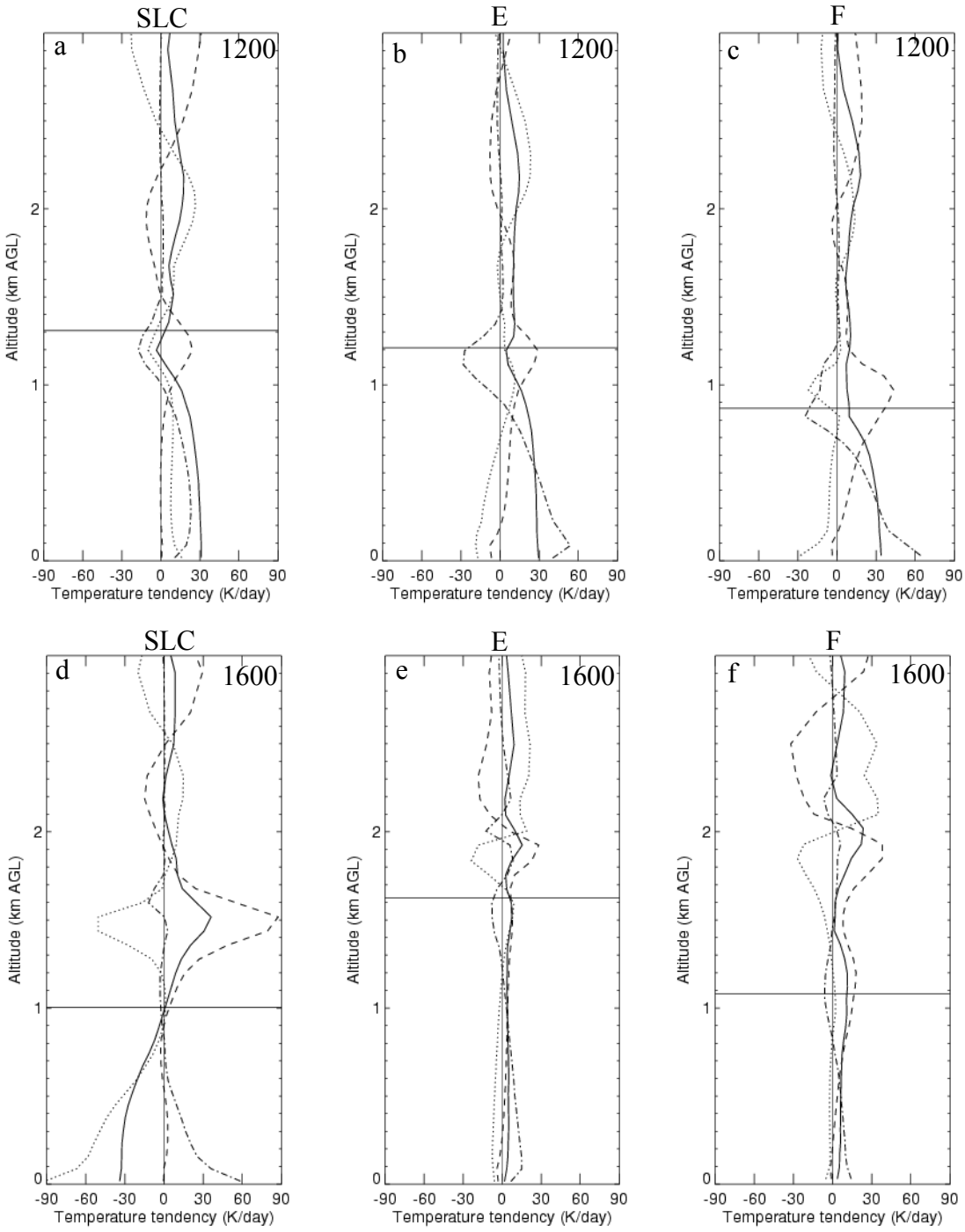

Fig. 2.13. Components of the temperature tendency equation at 1200 LST at (a) SLC, (b) E, and (c) F; and at 1600 LST at (d) SLC, (e) E, and (f) F. Solid line indicates total temperature tendency; dotted line is horizontal advection; dashed line is vertical advection; and dash-dot line is turbulent flux divergence. Horizontal bars indicate the CBL top.

depth at SLC. At E, the CBL continues to develop in a more classical manner. It is only after surface heating has nearly ceased, just before sunset, that the CBL depth decreases dramatically at E and F (1700 LST, Fig. 2.11a). Surface temperatures begin to fall at this time, shutting off buoyant convection and causing the stability regime to change from free to forced convection.

The potential temperature tendency profiles are similar at E and F. However, subsidence warming near the CBL and cold air advection from the UV are both stronger at F than at E, contributing to the shallower CBL.

At 1700 LST, the LBF has passed SLC and is just over E (Fig. 2.12). The thermodynamic energy budgets of the three locations are presented in Fig. 2.14. Near the surface at SLC, once again horizontal cold air advection is countered but not balanced by turbulent heat flux convergence. At E, the atmosphere is cooling uniformly below ~1.5 km AGL because of horizontal advection near the surface and vertical advection (ascent) above 0.5 km AGL. At F, the CBL has collapsed and cooling at the surface is overlain by weak warming, contributing to continuing stabilization.

2.5 Discussion

The dominant mechanisms controlling the evolution of the CBL in the SLV during this case are the GSL lake breeze and downvalley cold air advection from the UV. The effect of cold air advection from the UV could have been exaggerated in the simulation because of inadequate representation of the Traverse Range. This narrow feature may be important in limiting exchange between the SLV and UV; if represented as a lower, broader ridge in the MM5 topography, it could result in an overestimate of the influence of Utah Lake in

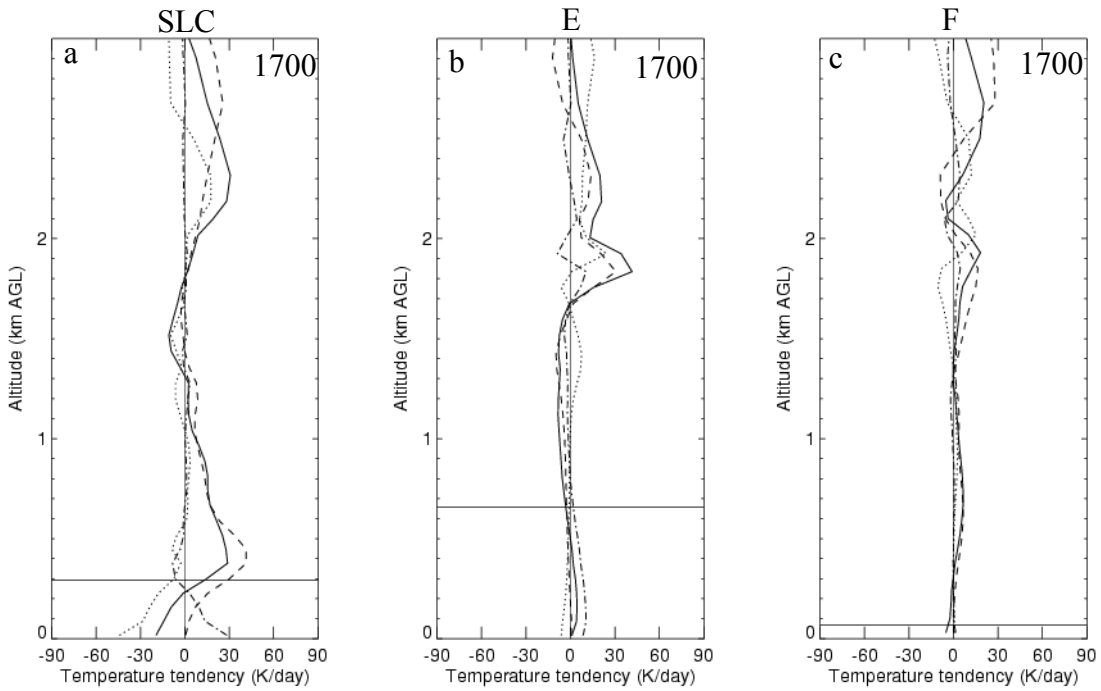

Fig. 2.14. Components of the temperature tendency equation at 1700 LST at (a) SLC, (b) E, and (c) F. Solid line indicates total temperature tendency; dotted line is horizontal advection; dashed line is vertical advection; and dash-dot line is turbulent flux divergence. Horizontal bars indicate the CBL top.

modulating valley and lake breeze flow in the SLV. In addition, differential surface heat flux divergence across land cover boundaries leads to persistent horizontal gradients in CBL depth throughout the day. In the afternoon, the CBL depth is decreased by subsidence warming aloft and horizontal cold air advection near the surface. These effects occur as a result of the slope of the SLV and the presence of the GSL and Utah Lake.

In the south end of the SLV, the maximum CBL depth is <1200 m, while in the middle of the SLV, the CBL grows to 1800 m deep. Advection of cold air from over Utah Lake in the UV allows a relatively shallow CBL to persist. The subsidence observed in the south end of the SLV is a product of cold air from the UV flowing down the inclined floor of the SLV, an effect perhaps overestimated because of model topography that does not capture the height of the Traverse Range. Low values of surface sensible heat flux over agricultural land in the southern SLV and cross-valley circulations related to slope flows on the valley sidewalls may also play an important role in generating subsidence in the south end of the SLV. Utah Lake acts as a cold air source throughout the day in this simulation, and it is only after the LBF from the GSL advances southward up the SLV that downvalley flow ceases. Lake temperature observations are not available for Utah Lake, so it is not clear to what extent it may contribute to such a phenomenon in the real world.

The north end of the SLV, in contrast, is characterized by the rapid local warming of urban surfaces and by the mid afternoon passage of the LBF. This creates favorable conditions for the afternoon intensification of the LBF and its subsequent movement up the SLV in the form of a classical sea breeze front, and is consistent with observations of sea breeze frontogenesis as discussed by Reible et al. (1993) and Simpson (1994).

Horizontal advection of lake boundary layer air from over the GSL contributes to a rapid decrease in CBL depth with the passage of the LBF. The highest CBL depths are observed just ahead of the LBF, where strong mass convergence and rising motion enhances turbulent heat flux convergence. In this study, in the north end of the SLV, the surface potential temperature tendency is dominated by advection of cold air from over the GSL with the passage of the LBF. In the south end of the valley, cold air advection contributes to keeping CBL depths lower than in the middle of the SLV. Between the lakes, the hot dry urban substrate is heated extensively and the CBL is able to deepen. Weigel (2005) hinted at the possible importance of horizontal cold advection near the surface in suppressing CBL depths in an Alpine valley, although subsidence was the dominant mechanism for CBL suppression in that case. The key differences between this study and Weigel (2005) are weaker solar heating (Weigel 2005 focused on a July scenario) and the presence of Utah Lake in the upper part of the SLV/UV system.

The transition time from downvalley to upvalley flow during the study period corresponds better to observations of lake and sea breezes (e.g., Simpson 1994) than to observations of valley winds (e.g., Weigel 2005). The wind shift occurs in the mid to late afternoon, rather than at midday, and behaves like a mobile front. The relative weakness of the October sun contributes to the lateness of the transition relative to other valley breeze studies. Most studies of daytime topographic flows take place in the summer months when the sun angle is high and the net radiation R_n is large.

A conceptual model of the SLV/UV wind system under weak synoptic forcing is presented in Fig. 2.15.The important features are the GSL, Utah Lake, the valley sidewalls, and the valley floor that slopes upward from the GSL to Utah Lake. This leads to strong

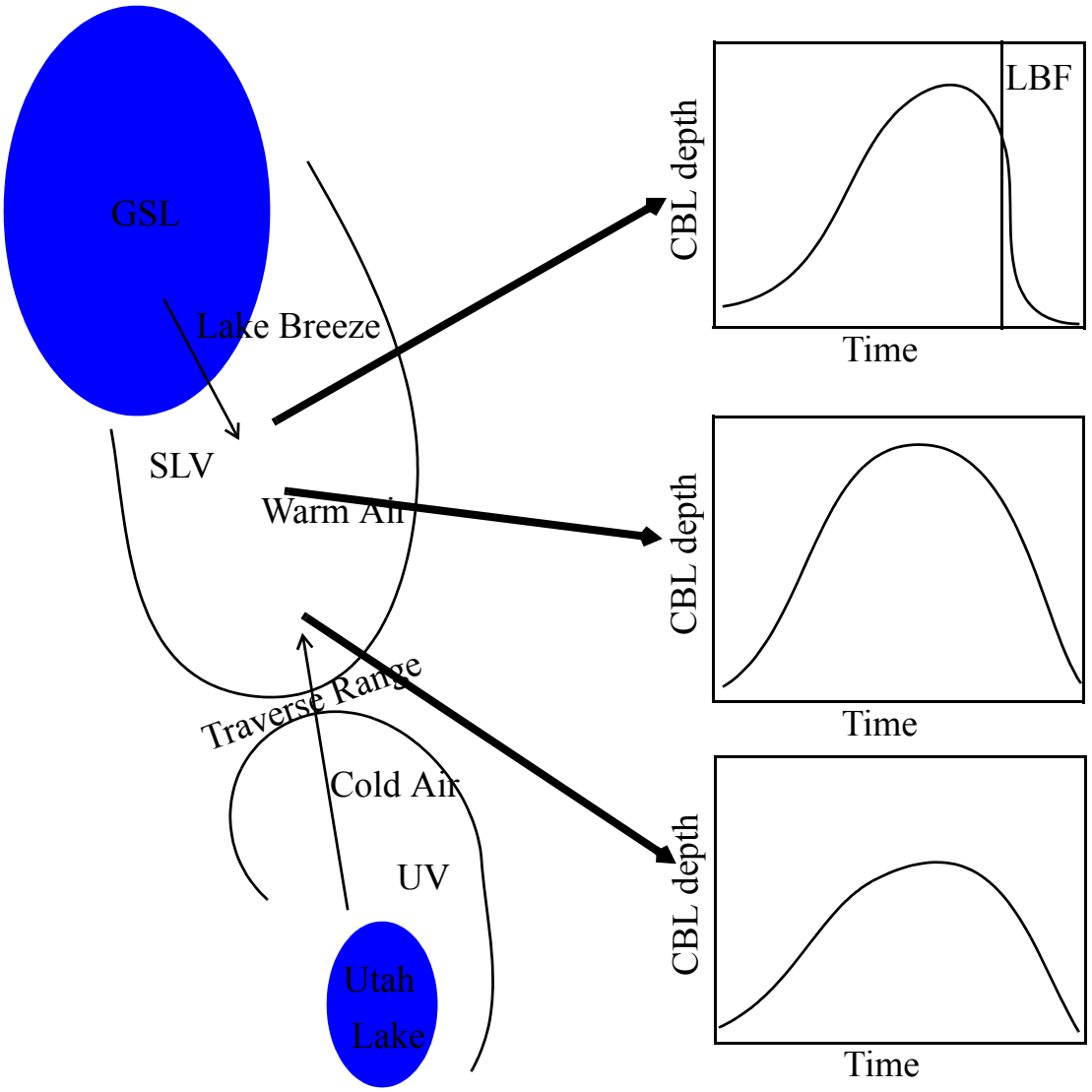

Fig. 2.15. Conceptual model of CBL evolution in the SLV, illustrating the role of the GSL, Utah Lake, and the warm urban area in the SLV.

downvalley flow in the morning, as the usual morning drainage flows combine with cold air advection from Utah Lake. Rapid heating of the urban areas in the central and northern portions of the SLV enhance mass convergence and reinforce downvalley flow between Utah Lake and the central SLV.

In the afternoon, the LBF gains ground against the deep southerly flow as the temperature gradient between the GSL and the SLV increases. Ahead of the LBF, the CBL is able to grow without inhibition (i.e., surface cold air advection does not contribute to CBL suppression). After the passage of the LBF, however, the CBL decreases dramatically. In locations where the LBF does not pass before surface heating has declined with sunset, the CBL evolves in a manner typical of flat surfaces.

2.6 Conclusions

The boundary layer structure for fair-weather simulations in the SLV showed heterogeneous spatial structures and complex evolution throughout the daytime. In some locations, convective heating of the valley atmosphere was opposed by horizontal cold air advection and mid-valley subsidence. These phenomena were diagnosed through an analysis of the thermodynamic energy budget. Surface cold air advection was evident by a dominance of the horizontal temperature advection term, while compensatory subsidence and lowering of the CBL top was characterized by heating from vertical advection (adiabatic warming). The advection of statically stable air from over the Great Salt Lake, in a manner similar to the CBL advection noted by Zhong and Doran (1995), was responsible for the rapid decrease in CBL depth as the lake breeze front passed.

This study has identified several challenges to improving air quality forecasts under anticyclonic conditions, during which forecast validation normally receives little attention. The gross features of diurnal circulations in complex terrain were well simulated, though it was found that Utah Lake played an unexpected and significant role in modulating the simulated CBL depth in the southern end of the SLV. The timing errors observed were a result of this factor as well as of discrepancies in surface characteristics and the limitations of model PBL representation. The influence of Utah Lake may have been overestimated due to the inadequate representation of the Traverse Range. The Traverse Range represents a significant barrier between the SLV and UV, broken only by the gap of the Jordan Narrows.

The most important items to verify are the surface characteristics of the SLV, which played a large role in producing the simulated CBL features. For example, the moisture availability of urban and natural land cover types could be substantially different from those specified here, depending on preceding weather conditions; the local behavior of the CBL, as well as the timing of up- and downvalley flow transitions, are directly related to these factors.

CHAPTER 3

EFFECTS OF URBANIZATION AND IRRIGATION ON THE METEOROLOGY OF THE SALT LAKE AND UTAH VALLEYS UNDER ANTICYCLONIC CONDITIONS

3.1 Introduction

Land cover change is an inevitable consequence of human habitation that can have significant impacts on air quality and surface temperatures. The urban heat island is one example of how land cover change can affect atmospheric processes with implications for human health and comfort. Nocturnal minimum temperatures can be as much as 12° C warmer in urban areas than surrounding rural areas (Oke 1995), a potentially hazardous situation during heat waves, particularly for vulnerable people. In addition, higher urban temperatures also increase energy consumption and can strain utility services (Sailor 1995).

Because of turbulent mixing, the effects of land cover change can extend through the boundary layer (Oke 1982). Changes to mixing depths can affect surface pollutant concentrations, sometimes resulting in degraded air quality and respiratory problems for the elderly and infirm. Local circulations and moisture fluxes may be altered by urban and agricultural land cover transformations, with consequences for the distribution of precipi-

tation (Huff and Changnon 1973; Diem and Brown 2002; Shephard and Burian 2003). Quantifying the effects of land cover change on atmospheric processes can lead to better-informed decision making in matters of urban planning and other public policy issues.

The implications of land cover change on atmospheric processes depend on the nature of the change and the climatic context in which it occurs. For example, deforestation in a humid environment has a drying and warming effect, whereas irrigated agriculture in a desert region moistens and cools the local atmosphere (e.g., Souza et al. 2000; Diem and Brown 2003). Land cover change can have a significant influence on locally driven circulations such as sea breezes and mountain winds (e.g., Yoshikado 1992; Marshall et al. 2004). This study focuses on urbanization and agricultural development in a semi-arid mountain valley, where local thermally driven flows drive transport and mixing on many days. The term planetary boundary layer (PBL) will be used to describe a layer between the surface and the top of a mixing layer generically, while the term convective boundary layer (CBL) describes specifically a daytime mixing layer driven by buoyant convection. The depth of the CBL is used as an indicator of the integrated effects of land cover change, as it takes into account the horizontal and vertical redistribution of heat by boundary layer processes.

Diurnal thermally driven flows are generated by surface heat flux contrasts. These arise from sloping terrain, land/sea boundaries, and other land cover heterogeneities such as irrigated land patches in arid surroundings. Because cities are often located in valleys and on coastlines, interactions between thermally driven circulations are commonly observed and important for human populations. These types of interactions have been examined in a variety of scenarios. Urban and sea breezes can produce synergistic circula-

tions leading to enhanced inland pollutant transport (e.g., Ohashi and Kida 2002). Kitada et al. (1998) and Yoshikado and Tsuchida (1996) demonstrated that an urban area could enhance surface convergence zones generated by the sea breeze and topographic flows. Schultz and Warner (1982) found that the Los Angeles urban area exerted little influence on the more dominant sea breeze and topographic flows, while Stivari et al. (2003) concluded that land cover flows did have a noticeable effect on the observed lake breeze.

Zhong and Doran (1995) suggested that simulated land cover flows may be overestimated in many cases because of the patchy and heterogeneous nature of most real landscapes, but they also found that mesoscale heat and momentum fluxes can have an important impact on local meteorology, especially on the CBL depth, a finding reinforced by Baidya Roy et al. (2003). In addition, synoptic winds sometimes interact with mesoscale heat fluxes to produce unexpected results. For example, Zhong and Doran (1995) observed a deeper CBL over a patch of irrigated farmland than would be predicted by the local surface sensible heat flux. A deep CBL had been advected by synoptic-scale winds from over a nearby arid steppe region. The surface temperatures over the two land cover types did reflect the local surface sensible heat flux differences; CBL depths did not. Zhong and Doran (1995) concluded that while land cover changes may only have small impacts on the mesoscale fluxes in a domain, some important local parameters like surface temperature and CBL depth may be strongly affected.

Prior to the arrival of European settlers starting in 1847, the predominant valley land cover type in the Salt Lake Valley (SLV) was grassland (Cottam 1947). The landscape has been transformed by the planting and irrigation of crops, grazing of cows and sheep, and urban settlement. This study addresses the question of how, for a given scenario with weak

synoptic forcing (i.e., light winds and clear skies), local-scale landscape changes have affected the transport and mixing of heat, momentum, and pollutants in the SLV and adjacent Utah Valley (UV). The next chapter outlines the approach taken to address this question, results are presented in chapter 3.3 and discussed in chapter 3.4, and conclusions are drawn in chapter 3.5.

3.2 Methodology

This study comprises two simulations using the Pennsylvania State University (PSU)/ National Center for Atmospheric Research (NCAR) fifth-generation Mesoscale Model (MM5). Both simulations were initialized using the National Centers for Environmental Prediction (NCEP) Eta model (Black 1994; Rogers et al. 1995, 1996) analysis at 0000 UTC 16 October 2000, and run for the day preceding Intensive Observing Period 6 (IOP6) of the Vertical Transport and Mixing Experiment (VTMX, see Doran et al. 2002), hereafter referred to as "the study period". Fig. 3.1 gives an overview of the relevant locations for this chapter. The first simulation, described in detail in section 2.2, uses the United States Geological Survey (USGS) National Land Cover Data (NLCD) 1992 database (Vogelmann et al. 2001), and is referred to in this chapter as the 1992 run. The USGS NLCD is the most recent dataset readily available with 1 km resolution and multiple urban land cover classes. Due to continuing rapid urban growth, this may still underestimate the actual urban land coverage along the Wasatch Front during the study period. The second simulation is identical to the first except that all urban and agricultural land cover types were replaced by grassland. This simulation is termed the 1847 run. Figure 3.2 shows the land cover in the Wasatch Front region of northern Utah, including the SLV and UV, for

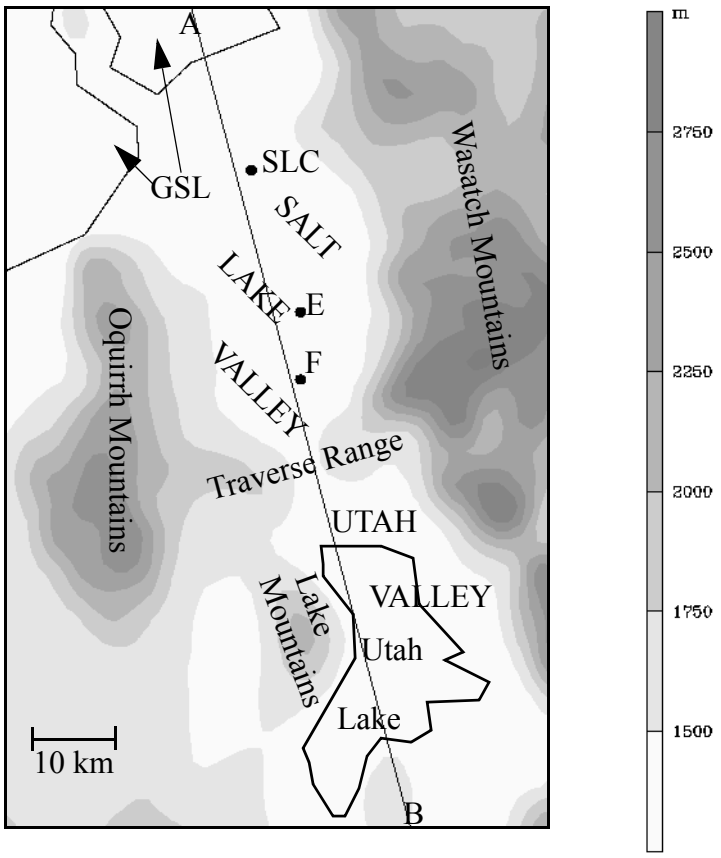

Fig. 3.1. Topography and important locations in the SLV. SLC is the Salt Lake City International Airport; E and F are valley-bottom analysis locations. SLC, E, and F are in the SLV; Utah Lake is in the UV. A and B are endpoints of cross section presented in later figures.

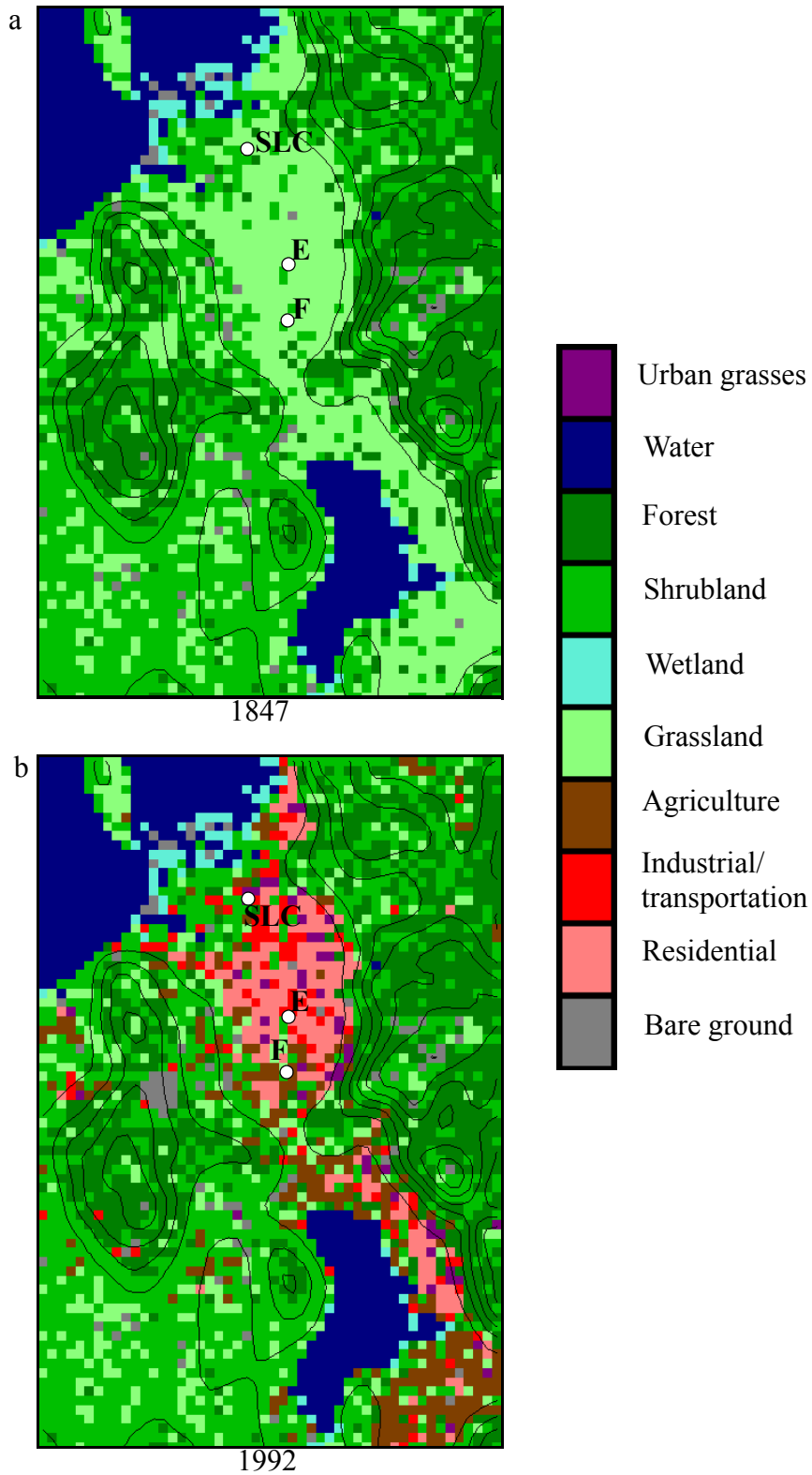

Fig. 3.2. Land cover and topography in the SLV for pre-settlement (1847) and urban (1992) simulation. Topography contour interval is 250 m. Important locations marked.

the 1847 and 1992 runs. The SLV in the 1847 run is dominated by grassland, with a few grid cells of shrubland and bare ground. In the 1992 simulation, a mosaic of urban and natural land cover types blanket the central SLV, and there are extensive agricultural areas in the southern SLV. The UV is dominated by the presence of Utah Lake, which is surrounded in the 1847 run by grassland and shrubland. In the 1992 run, the eastern UV is composed of mostly urban land, while the northern and southern ends of the UV are predominantly agricultural. The western UV is mostly natural land cover and contains the Lake Mountains. Table 3.1 presents characteristics of the common land cover types along the Wasatch Front. Natural land cover types are denoted by an "N"; agricultural or other non-urban anthropogenic types are denoted by an "A"; urban land cover types are denoted by a "U".

Table 4: Land cover characteristics

Land cover	Moisture availability (fraction)	Heat capacity ($MJ\ m^{-3}\ K^{-1}$)	Roughness length (m)	Albedo (fraction)	Thermal inertia ($J\ m^{-2}\ K^{-1}\ s^{-1/2}$)
Grassland (N)	0.15	2.08	0.1	0.23	1675
Shrubland (N)	0.10	2.08	0.1	0.25	1675
Cropland (A)	0.50	2.50	0.05	0.23	1675
Wetland (N)	0.75	2.92	0.2	0.14	2513
Open water (N)	1.00	-NA-	10^{-4}	0.08	2513
Bare ground (N/A)	0.05	1.20	0.1	0.25	837
Forest (N)	0.60	2.92	0.2	0.14	2094
Residential (U)	0.10	1.89	0.91	0.15	1256
Urban grass (U)	0.30	2.08	0.1	0.23	1675
Commercial/ industrial (U)	0.10	1.89	1.08	0.15	1256

No allowances were made for elevation dependence or other factors that might affect land cover, e.g., the replacement of native grassland with shrubland as a result of intense grazing by sheep and cows (Stewart 1941). This was considered an appropriate strategy for two reasons. First, urban and agricultural lands are found in valleys and have most likely replaced grasslands, and not other land cover types like evergreen forest, which is more common at higher elevations. Second, compared to the differences between natural land cover types (grass- and shrubland) and the urban and agricultural land cover types that replace them, the differences between shrubland and grassland are small.

The characteristics of the land cover types were set to default MM5 settings for the cool season, with two exceptions. Roughness lengths for the urban categories were specified according to Burian et al. (2002). Second, moisture availability values for grassland and shrubland were decreased relative to the default values to more closely simulate the semi-arid conditions of the region. This resulted in simulated Bowen ratios that were consistent with those reported by Malek and Bingham (1997) and Ivans (2005). The thermal and radiative characteristics of the urban land cover classes yield Bowen ratios consistent with observations in Phoenix, AZ (Grimmond and Oke 1995). The land cover datasets used represent our best guesses of the land cover types and characteristics along the Wasatch Front in 1847 and 1992.

Validation of the 1992 model run is described in Chapter 2 of this dissertation. Despite some known limitations (e.g., moisture availability contrasts between urban, natural, and agricultural areas may not be representative of the real situation in the SLV), the model adequately simulates the temperature, wind, and CBL structure over the SLV.

3.3 Results

The study period on 16 October 2000 was characterized by clear skies and weak crest level (700 hPa) winds, allowing thermally driven flows to develop. At 1200 LST, the 1992 simulation produces surface temperatures up to 2°C greater than in the 1847 simulation (Fig. 3.3a) and the CBL is up to 300 m deeper (Fig. 3.3b). Because difference fields are calculated as (1992 run) - (1847 run), comparative terms such as "warmer" and "deeper" will refer to the 1992 run relative to the 1847 run, unless otherwise specified. The largest differences occur on the east side of the SLV, where there is a large area of contiguous urban land in the 1992 simulation (see Fig. 3.2). Analysis of difference wind vectors reveals that there is increased mass convergence over the eastern SLV. An examination of the surface energy budget reveals that increased urban heating in the 1992 simulation is responsible. At E, the maximum sensible heat flux in the 1992 simulation is ~50 W m^{-2} higher than in the 1847 simulation (Fig. 3.4b), while other components of the surface energy budget are similar. The lower albedo of the urban surface leads to higher values of net radiation R_n and surface sensible heat flux. This results in the observed increase in convergence over the heated area.

At SLC, on the other hand, latent heat flux is larger in 1992. At F, latent heat flux is also higher in 1992, owing to the larger moisture availability of the irrigated agricultural land there. Because the net radiation is nearly the same for both of these locations, the increase in latent heat flux is balanced by a decrease in the sensible heat flux.

A vertical cross section along the line A-B (see Fig. 3.1 for location) shows the difference fields of θ and vertical velocity, and difference vectors of wind in the plane of the cross section (Fig. 3.5). The warm anomaly over the urban areas of the central SLV is evi-

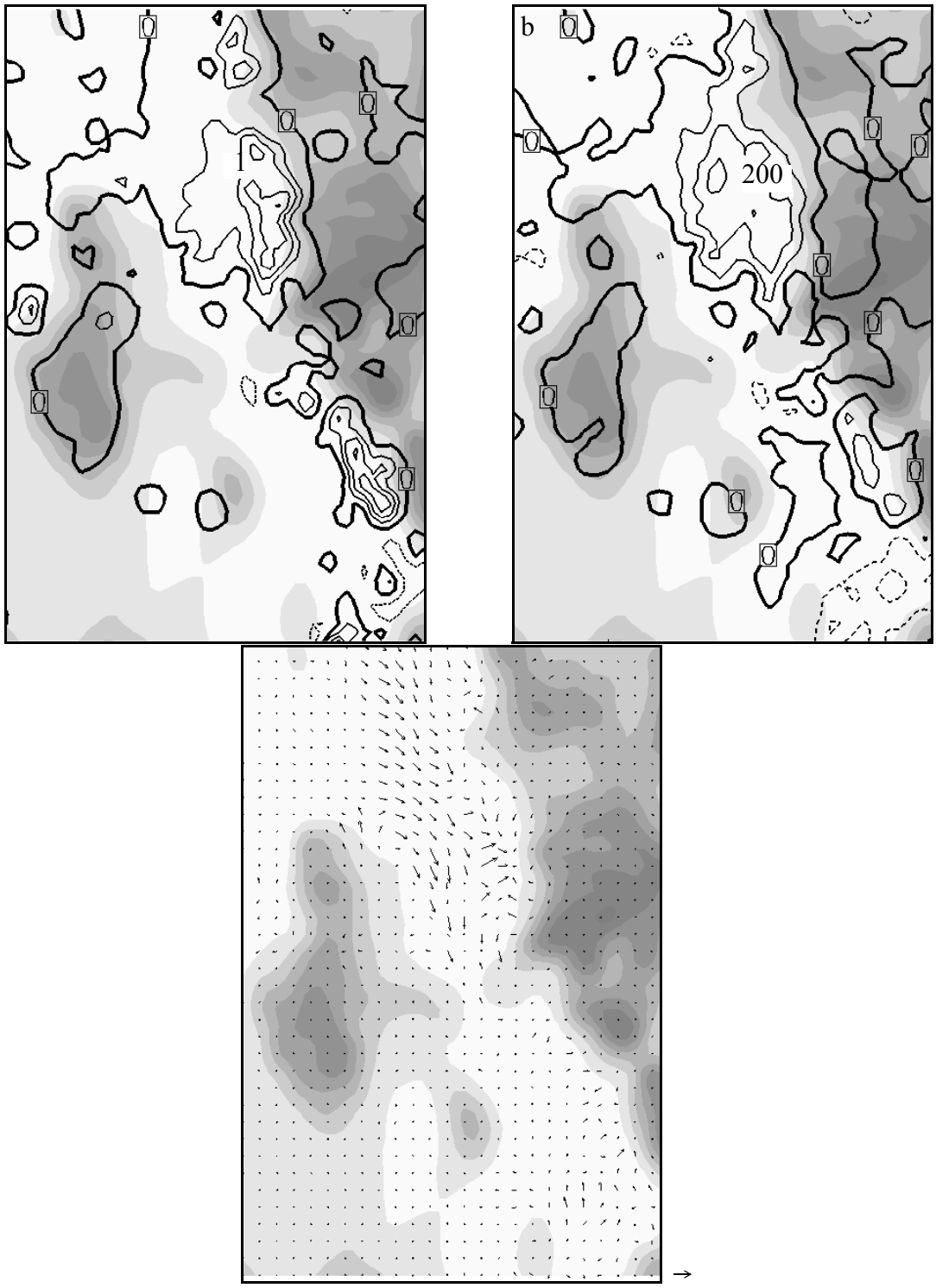

Fig. 3.3. Difference fields (1992 - 1847) at 1200 LST, of (a) temperature (°C), (b) CBL depth, and (c) wind vectors. Contour interval is 0.5°C for (a) and 100 m for (b); zero contours in bold, negative contours are dashed. Reference vector in lower right is 1 m s^{-1}.

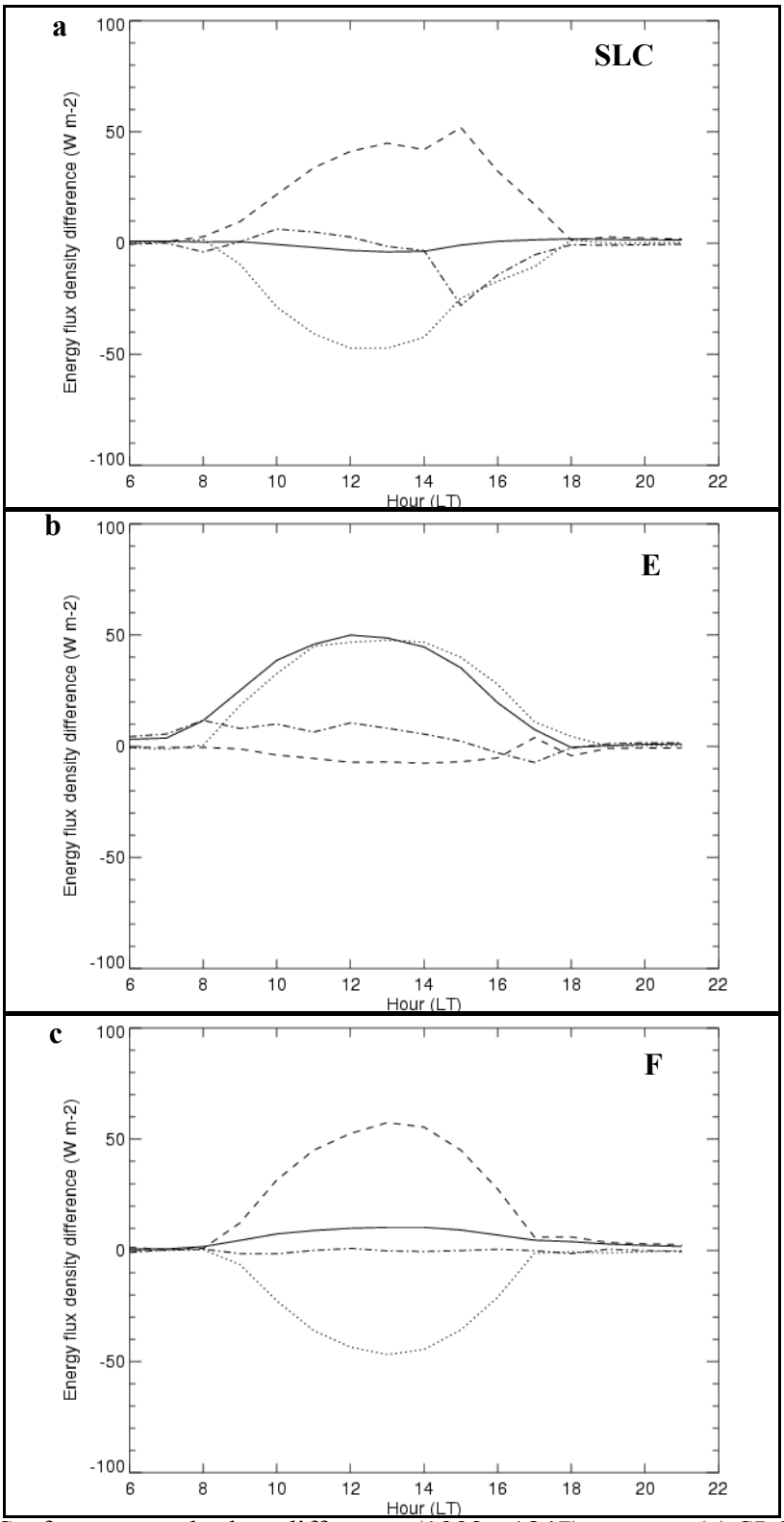

Fig. 3.4. Surface energy budget difference (1992 - 1847) terms at (a) SLC, (b) E, and (c) F. Solid lines are net radiation; dotted lines are sensible heat flux; dashed lines are latent heat flux; and dash-dot lines are ground heat flux.

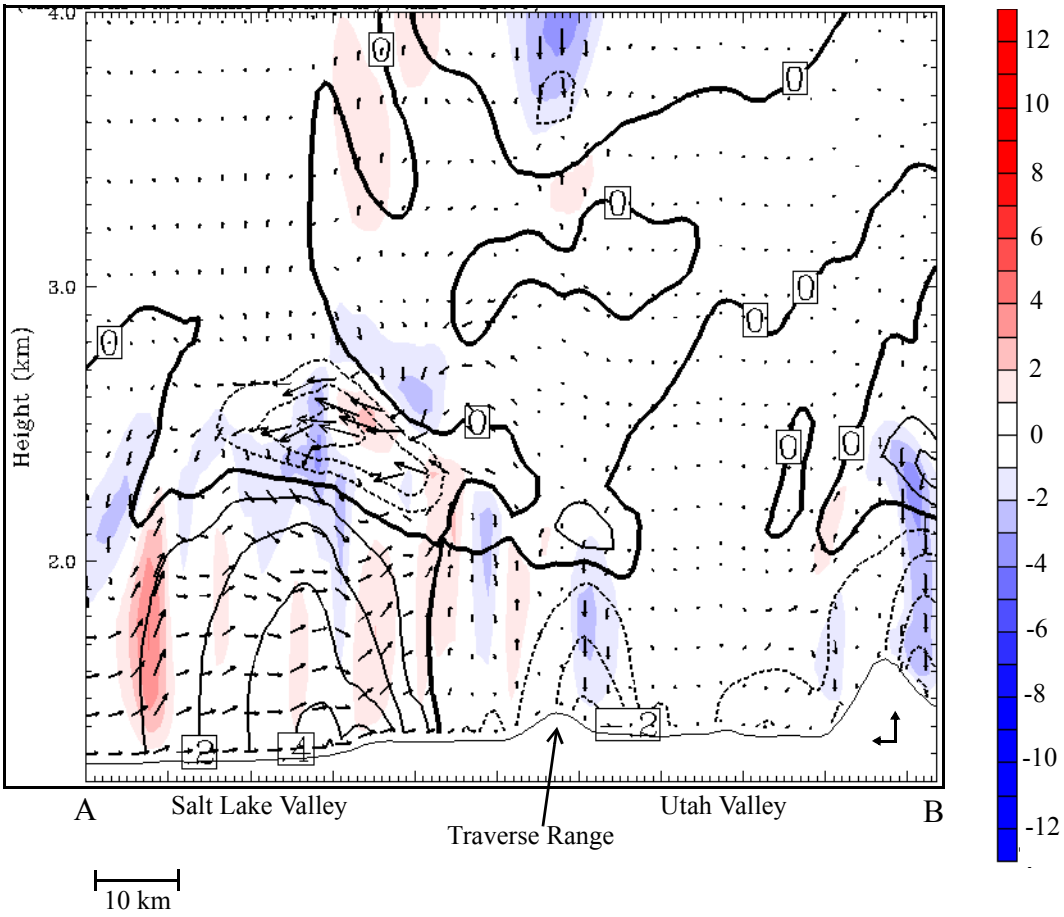

Fig. 3.5. Difference fields (1992 - 1847) at 1200 LST, of potential temperature (K), vertical velocity, and circulation vectors along cross section A-B. Reference vectors in lower right are 1 m s^{-1} horizontal and 3.5 cm s^{-1} vertical. Colorbar indicates vertical velocity in cm s^{-1}.

dent, along with enhanced southerly flow aloft. There is also a cold anomaly near the Traverse Range, associated lower values of sensible heat flux, a result of local surface energy balance differences.

In the afternoon (1500 LST), three different effects of land cover change are evident (Figure 3.6). First, surface temperatures and CBL depths in 1992 are lower in the south end of the SLV and the northern and southeastern portions of the UV. These are regions where the land cover is grassland in 1847 and agricultural land in 1992, with the primary difference being the higher soil moisture availability of the irrigated agricultural land.

Second, surface temperatures and CBL depths in the eastern SLV are greater in 1992 than in 1847, although the difference is less than at 1200 LST (cf. Figs. 3.3, 3.5).

Third, there is a region of lower CBL depths in the northeast portion of the SLV (Fig. 3.6b) that is related to the more rapid advancement of the lake breeze front (LBF) associated with the GSL. The land cover in the region with lower CBL depths does not differ greatly between the simulations, indicating that this is a nonlocal effect of land cover change.

A cross section along A-B at 1500 LST (Fig. 3.7) reveals the nonlocal effects of the accelerated LBF. This is shown by the updraft/downdraft couplet centered at 25 km, indicating that the LBF updraft in 1992 is south of that in 1847. The warm anomaly and weak upward vertical velocities associated with the urban area at 1200 LST have been overwhelmed by the LBF effect, while the cold anomaly near the Traverse Range persists.

By 1700 LST, difference vectors of the surface wind (Fig. 3.8c) reveal that the 1992 LBF continues to accelerate into the eastern SLV, but its progress has been retarded in the western SLV. This deceleration is evident in a cross section along A-B (Fig. 3.9), in which

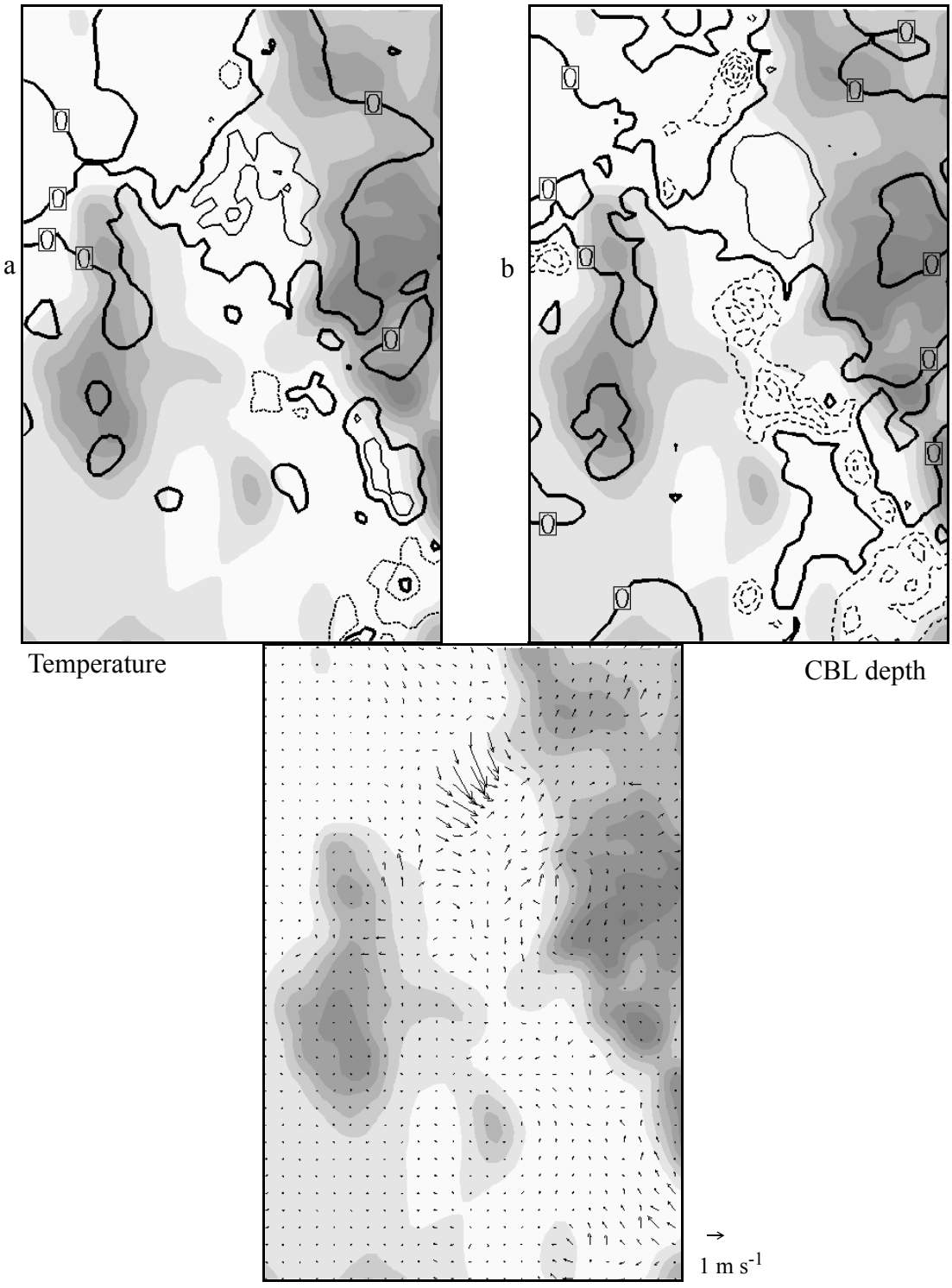

Fig. 3.6. Same as Fig. 3.3 except at 1500 LST.

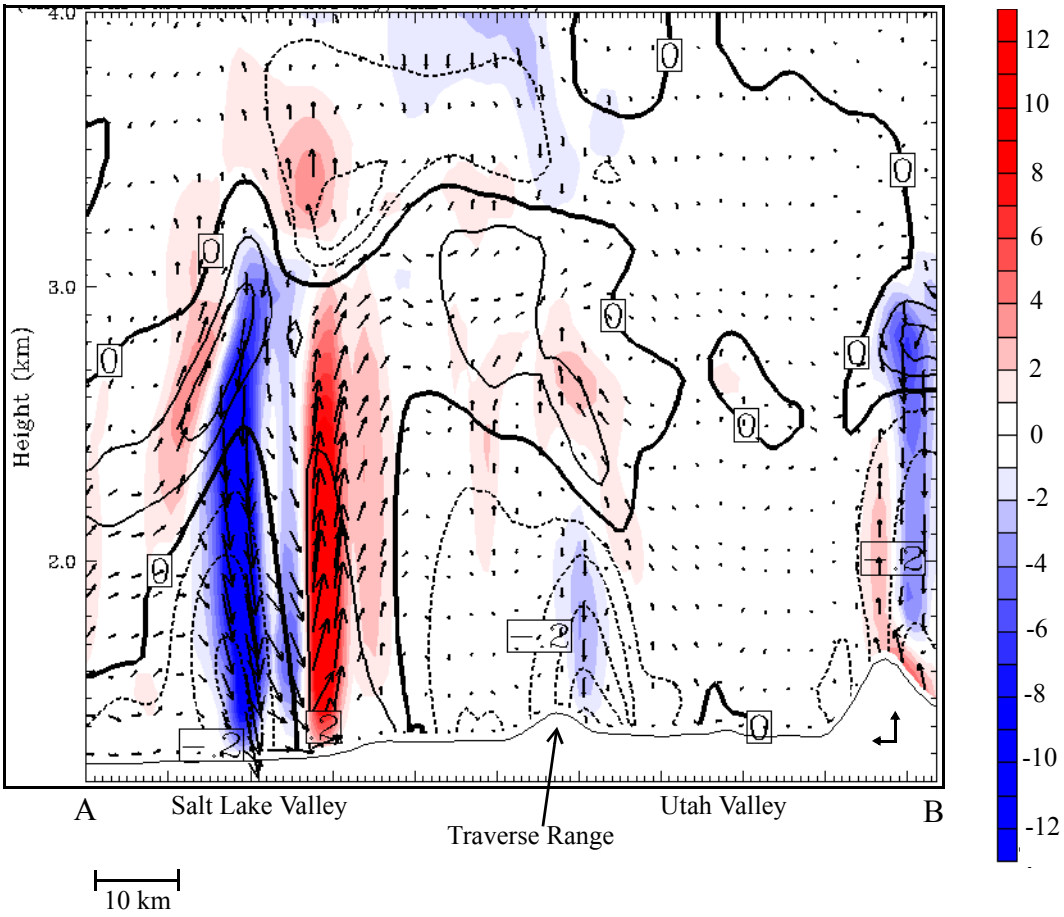

Fig. 3.7. Same as Fig. 3.5 except at 1500 LST.

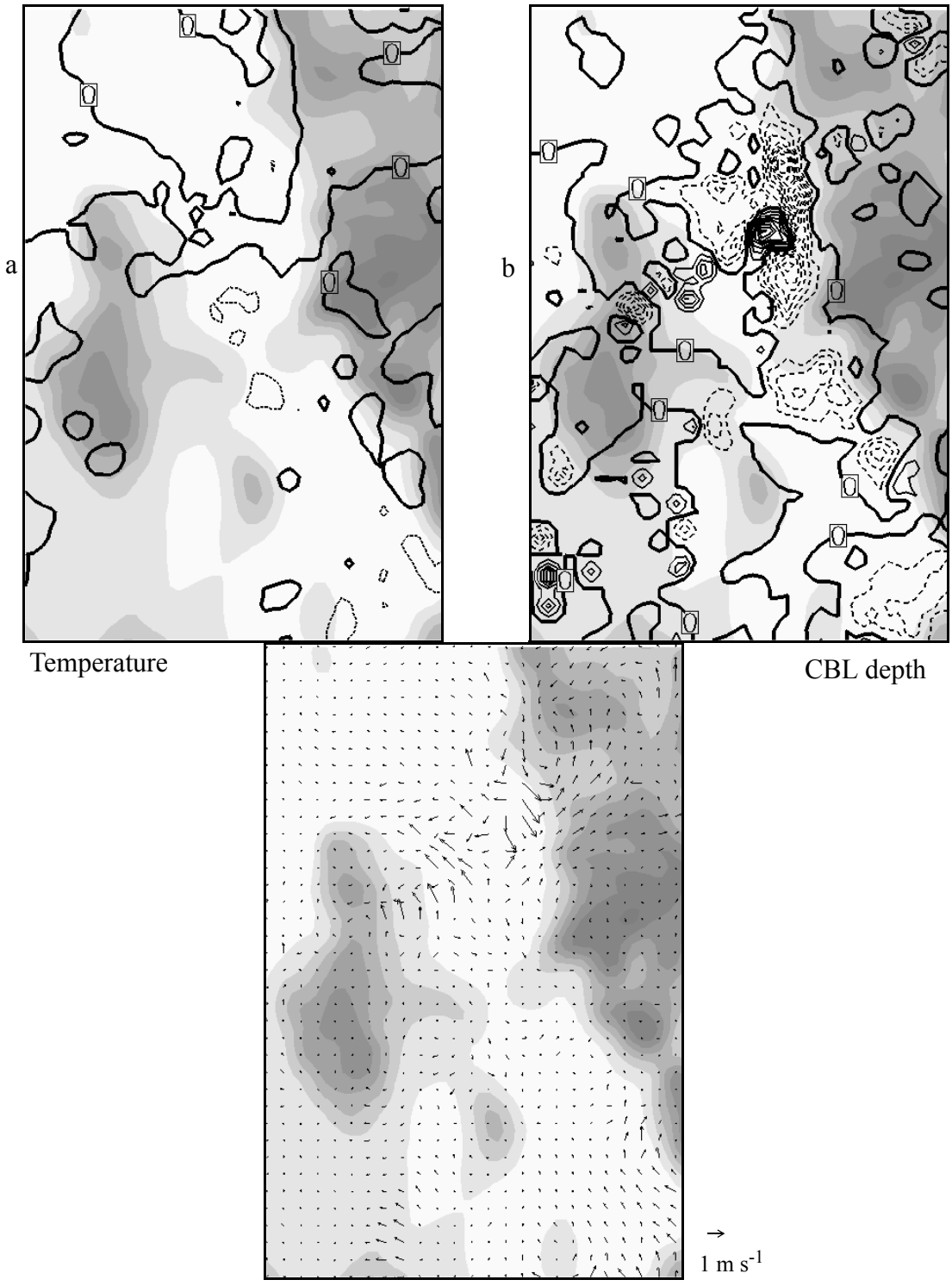

Fig. 3.8. Same as Fig. 3.3 except at 1700 LST.

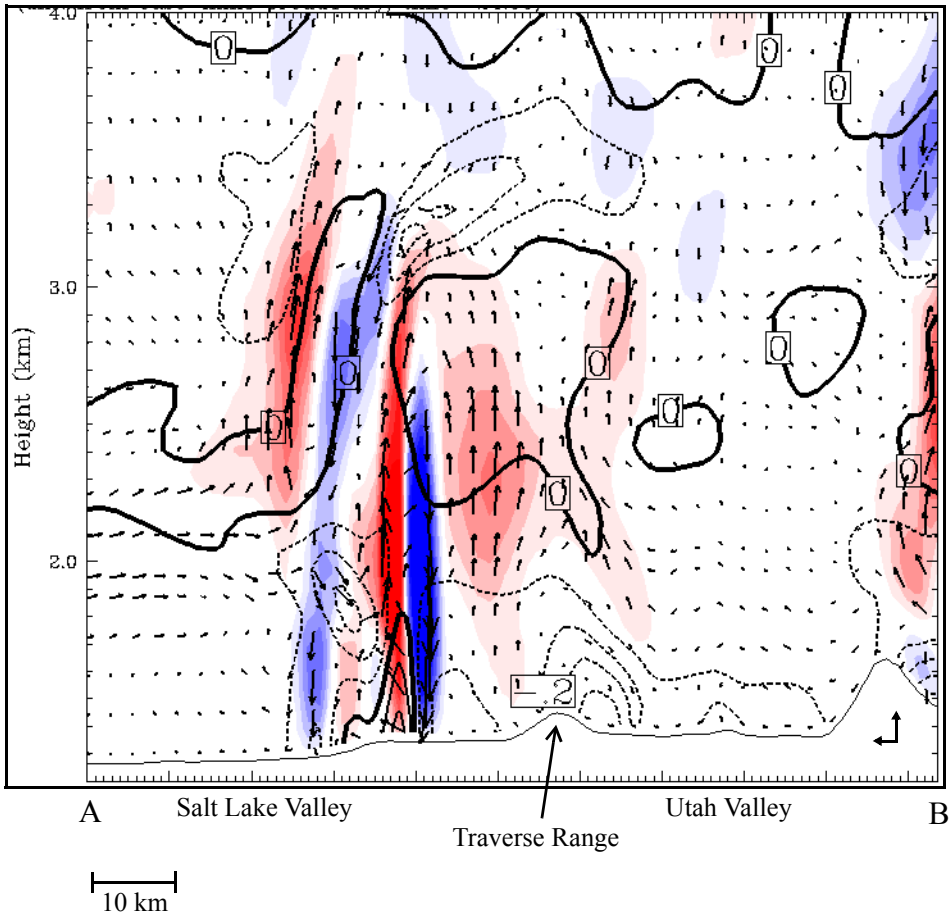

Fig. 3.9. Same as Fig. 3.5 except at 1700 LST.

the updraft-downdraft couplet observed at 1500 LST has been reversed. The surface temperature and CBL depth difference fields are complex and difficult to interpret (Fig. 3.8a,b).

Time series of CBL depth at three sites (SLC, E, and F) for both the 1992 and 1847 simulations are presented in Fig. 3.10. These time series illustrate several different effects of land cover change on the meteorology in the study area. In the 1992 scenario, SLC is surrounded by industrial land and urban grasses. E is in the southwest end of the largest contiguous block of urban land in the SLV, with agricultural and natural land several kilometers to the south and west. F is surrounded by agricultural and natural vegetation. In the 1847 scenario, all three sites lie in large tracts of grassland. SLC and F have higher soil moisture availability in 1992 than in 1847, while at E, it is virtually unchanged. However, at E, the albedo in the 1992 scenario is substantially lower than in the 1847 scenario.

At SLC, the difference in peak CBL depth between the simulations is less than 100 m. However, the CBL collapses rapidly after 1500 LST in the 1992 simulation, while it declines more slowly in the 1847 simulation. The LBF passes SLC earlier in the 1992 simulation than in the 1847 simulation, triggering the rapid mid afternoon collapse. The effect of LBF passage on the thermodynamic energy budget at 1500 LST is shown in Fig. 3.11. In the 1847 simulation, the heating rate is uniform throughout the lower CBL (Fig. 3.11a). In the 1992 simulation, however, the LBF has just passed SLC, and strong cold air advection at the surface is partly balanced by turbulent heat flux (Fig. 3.11b). The passage of the LBF at SLC is also evident as a spike in surface latent heat flux at 1500 LST (Fig. 3.4a). In the next hour, the CBL remains deep in the 1847 simulation, whereas it collapsed following the passage of the LBF in 1992 (Fig. 3.10a).

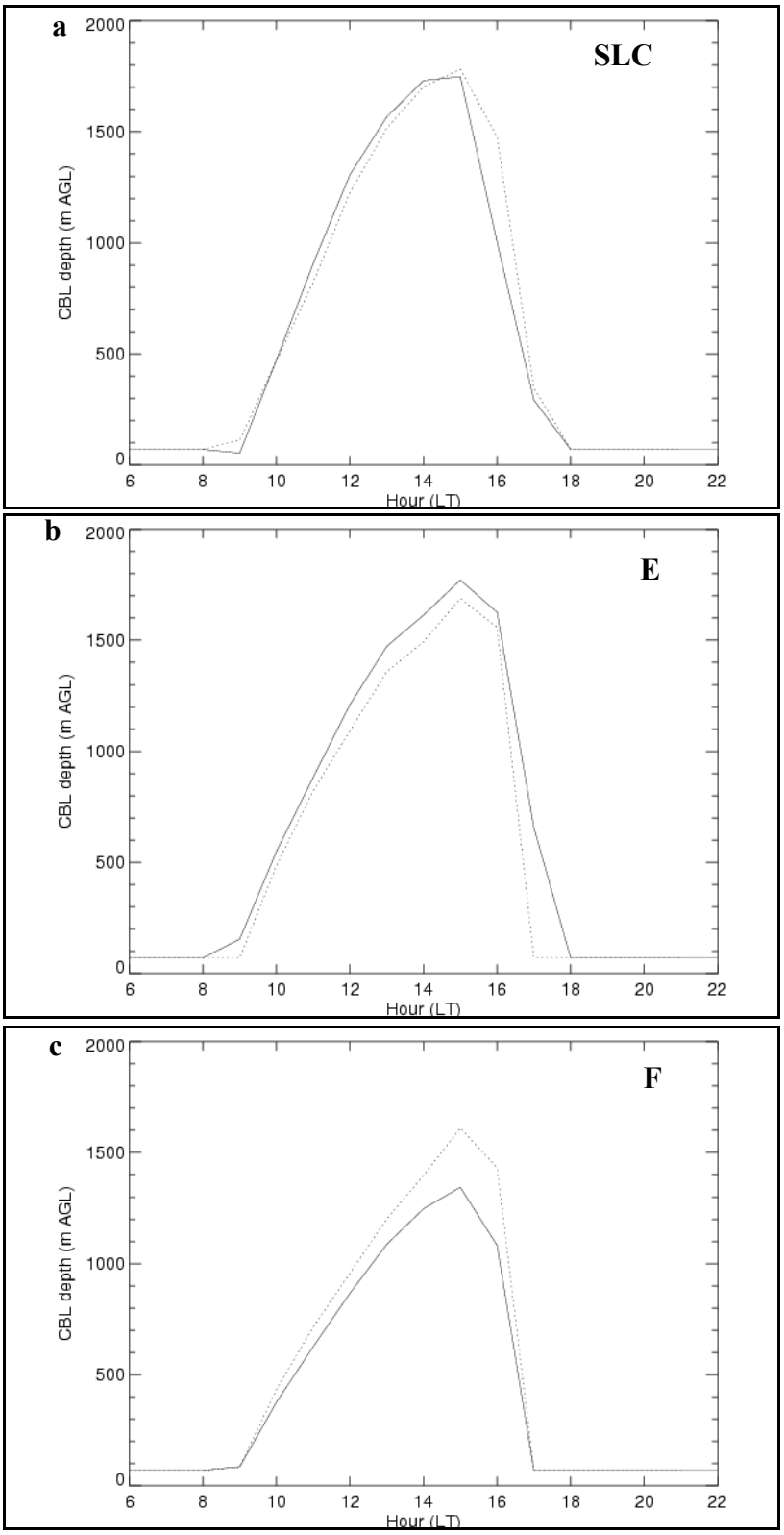

Fig. 3.10. Convective boundary layer depths at (a) SLC, (b) point E, and (c) point F. Solid lines are 1992; dotted lines are 1847.

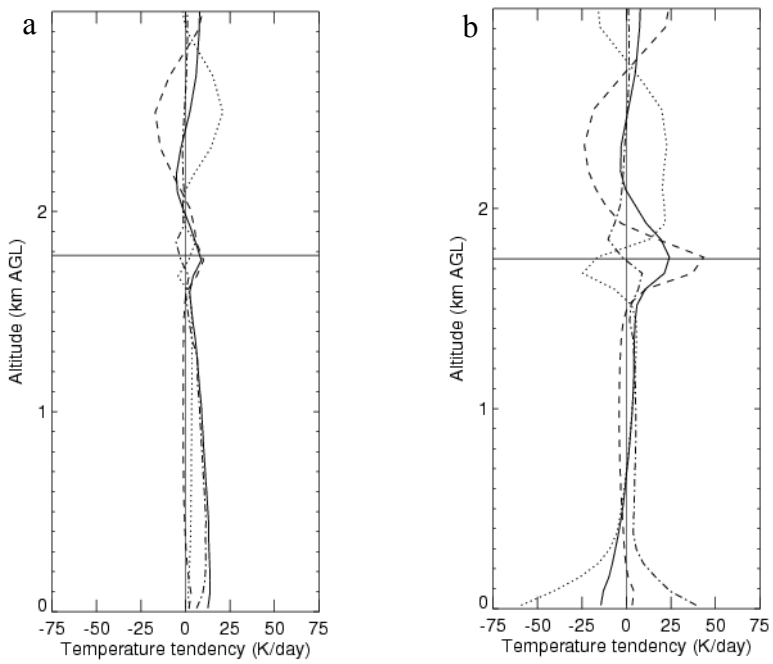

Fig. 3.11. Components of the potential temperature tendency equation at SLC at 1500 LST for (a) 1847 and (b) 1992. The solid line indicates the total potential tendency term; dotted line is the horizontal advection term; dashed line is vertical advection term; and dash-dot is turbulent term. The horizontal bar indicates the CBL top.

At E, the CBL in 1992 grows more quickly in the morning, and stays deeper longer in the evening, than in 1847 (Fig. 3.10b). Although the CBL in 1992 is deeper than in 1847 throughout the day, the difference is always <100 m. The differences observed can be attributed to the higher sensible heat flux in 1992 (Fig. 3.4b), a result of the lower albedo. This results in greater turbulent heat flux convergence at 1500 LST (Fig. 3.12a,b), though it is partly countered by cold air advection to yield comparable potential temperature tendency values and a relatively modest difference in CBL depth between the simulations. The later CBL collapse in 1992 can also be attributed to the higher surface sensible heat flux, which allows the CBL to remain deep at 1700 LST although the total heating rate is very similar to that in 1847 (cf. Figs. 3.12c,d).

At F, the CBL is shallower in 1992 than in 1847 throughout the day (Fig. 3.10c). The higher soil moisture availability in 1992, due to the irrigated agricultural land, yields lower sensible heat flux relative to 1847 (Fig. 3.4c). Another result of this difference is the lower surface temperatures observed near F in the afternoon (Fig. 3.6a).

The progression of the LBF in the SLV for the 1847 and 1992 simulations is summarized in Fig. 3.13. It shows that, during the mid-afternoon (1400-1600 LST), the LBF moves more quickly into the eastern SLV (where most of the urban land is concentrated) in the 1992 simulation than in the 1847 simulation. After that, the LBF positions in 1847 and 1992 become more coincident. This difference can be attributed to the lower albedo of the urban areas in 1992 than the grasslands that prevail in 1847. Greater sensible heat fluxes over the urban land result in a greater temperature difference between the air over the land and the air over the GSL. Increased horizontal temperature gradients (and hence density gradients) lead to more rapid LBF movement [expand] (Simpson 1994).

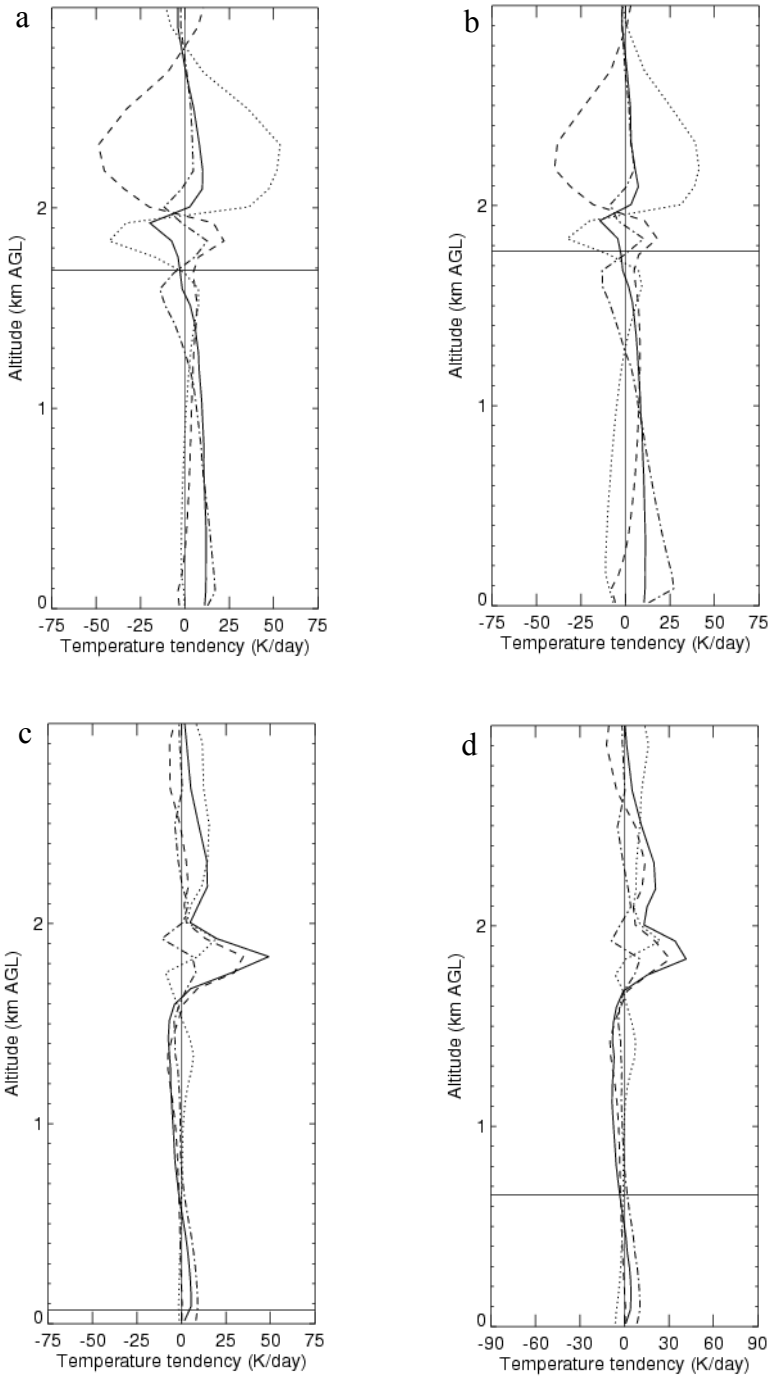

Fig. 3.12. Components of the potential temperature tendency equation at Point E at 1500 LST for (a) 1847 and (b) 1992, and at 1700 LST for (c) 1847 and (d) 1992. Solid line is the total potential temperature tendency term; dotted line is horizontal advection; dashed line is vertical advection; dash-dot line is turbulence. The horizontal bar indicates the top of the CBL.

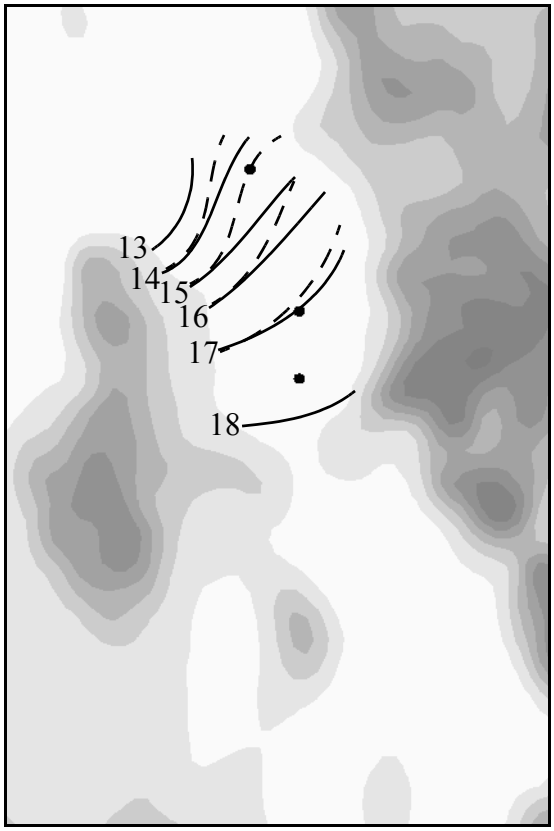

Fig. 3.13. Isochrones of the lake breeze front from 1200 to 1800 LST. SLC, E, and F are denoted by the bullets, but labels have been omitted for clarity. 1847 isochrones are dashed; 1992 isochrones are solid. Where only one isochrone is drawn, no appreciable difference between LBF positions existed.

3.4 Discussion

Anthropogenic land cover change along the Wasatch Front has comprised two disparate processes: urbanization and agricultural transformation. Compared to the natural land cover of the region, urbanization in the MM5 runs yields an increase in roughness length and a decrease in albedo, while cultivation and irrigation associated with agriculture increase the amount of moisture available for evaporation. These differences in surface characteristics lead to both local and non-local changes to surface temperature and CBL depth along the Wasatch Front.

The CBL depths in the simulations presented here exhibit two distinct changes with respect to land cover change. First, the timing of CBL development and collapse is determined by increases in net radiation arising from changes to albedo, and by the passage of the LBF. Second, the maximum CBL depth is controlled primarily by local moisture availability.

At SLC, the main difference in CBL evolution between 1847 and 1992 is in the timing of the afternoon CBL collapse. Locally, the land cover change represents an increase in surface moisture flux, suggesting that the CBL depth should be lower in 1992. However, the land-lake temperature difference is greater in the 1992 run because of the lower albedo of the urban land relative to the grassland prevalent in the 1847 run. As a result, the LBF passes SLC sooner in the 1992 run. The CBL depth decreases dramatically with the passage of the LBF as cold boundary layer air from over the GSL is advected through. In the 1847 run, by contrast, the LBF does not pass SLC until the CBL has already collapsed as a result of the decreasing surface sensible heat flux in the evening. The changes to CBL depth at SLC are driven by the non-local influence of the LBF.

At E, by contrast, local surface characteristics are responsible for the differences in CBL evolution between the 1992 and 1847 simulations. The lower albedo of the urban surfaces results in higher net radiation and hence higher surface sensible heat flux. The CBL grows more quickly and collapses later in the 1992 simulation, though the maximum CBL depth is only slightly greater. The LBF does not pass E until after the CBL depths have decreased as a result of radiative cooling; however, it is interesting to note that the movement of the LBF on the south and west sides of the urban area is retarded in the 1992 run relative to the 1847 run. The increased convergence over the urban area yields winds that accelerate the LBF north of the urban area, but slow it after it moves past the urban area.

At F, the increased moisture availability in the 1992 run yields lower values of surface sensible heat flux, and a shallower CBL throughout the day. Here, as at E, the CBL depth decreases as a result of radiative cooling long before the LBF passes. The replacement of natural land cover with irrigated agricultural land has a larger local impact on CBL depth than does urbanization, demonstrating the sensitivity of local circulations and boundary layer dynamics to moisture availability. However, the non-local impact of the altered LBF could have important consequences for locations near the GSL.

In addition to CBL effects, the urbanized area in the SLV displays a daytime urban heat island relative to the 1847 simulation, as the lower albedo of the urban surfaces leads to higher values of surface sensible heat flux. This is most prominent early in the day. Later on, the increased surface heating is distributed throughout the deep CBL and surface temperature differences decrease. Over agricultural areas in the 1992 simulation, afternoon surface temperatures remain lower throughout the afternoon relative to the natural

land cover in the 1847 run. Because agriculture in the semi-arid Wasatch Front region requires irrigation, an increase in surface latent heat flux and a locally low surface temperatures is imposed.

3.5 Conclusions

Sensitivity runs using the MM5 in a mountainous, semi-arid environment have identified surface characteristics that alter the behavior of the CBL and maximum surface temperatures. Urbanization of natural land cover types yields a decrease in albedo and consequent increase in surface sensible heat flux, while a transformation to irrigated agriculture decreases the surface sensible heat flux.

Urbanization was found to increase the net radiation during the daytime because of the decrease in albedo. This leads to increased surface temperatures and CBL depths, but has the additional impact of causing a convergent circulation. This convergent circulation affects the movement of the LBF through the SLV, accelerating it as it moves towards the urban area, and slowing it as it moves away.

The current development trend along the Wasatch Front involves the conversion of agricultural land to residential land. This transformation could yield more dramatic meteorological changes than the urban development of natural grass- and shrublands by compounding a loss in moisture availability with a decrease in albedo. This will produce a significant warming over those surfaces. In addition, the non-local effects of urbanization on the LBF could result in the CBL depths decreasing earlier in certain locations. The deceleration of the LBF in the southern and western SLV would be eliminated by the

urbanization of those areas. This process is already under way, as urbanization has continued since 1992, when the land cover database used here was collected.

The accurate specification of bulk surface characteristics is vital to producing high-quality forecasts of CBL depth in a semi-arid region of complex terrain such as the Wasatch Front. However, the largest uncertainties in this modeling study were related to the treatment of surface fluxes. Additional observation-based research is necessary to better quantify the energy balance over various land cover types along the Wasatch Front.

CHAPTER 4

CONCLUSIONS AND RECOMMENDATIONS

The dominant influences on surface temperatures and CBL depths during fair weather simulations along the Wasatch Front of northern Utah were found to be the GSL and Utah Lake. Although slope flows were also observed, divergence at the surface in the valley center as a result of slope flows on the valley sidewalls was not observed. Compensatory subsidence as a component of the cross-valley circulation was not considered to be an important factor in controlling the distribution of heat through the valley atmosphere. This contrasts with the findings of Rampanelli et al. (2004) and Weigel (2005). Large-scale subsidence was observed, but it was most likely the result of along-valley flow above the downward sloping valley floor rather than the result of the cross-valley circulation. Horizontal temperature advection and local land cover heterogeneities were responsible for the spatial and temporal patterns in surface temperature and CBL depth.

Particularly surprising was the influence of Utah Lake on the meteorology of the SLV. Cold air was found to drain northward into the SLV through the morning and into the afternoon and early evening. While the influence of Utah Lake is perhaps underappreciated, it may have been overestimated in this case. A more accurate representation of the Traverse Range may help to insulate the SLV from the UV and produce a more accurate simulation.

Sensitivity studies were conducted to determine the impact of land cover change on the case presented above. Both local and non-local effects of simulated land cover change were observed along the Wasatch Front. Local effects include changes to surface temperature and CBL depth as a result of the changes to the surface energy budget. Relative to natural grasslands, urban areas have a lower albedo, resulting in a higher R_n and higher surface sensible heat flux. Agricultural land has higher moisture availability and hence lower surface sensible heat flux. In the case of the urban areas, the morning surface temperatures and timing of CBL growth and decay were affected. Over irrigated agricultural land, surface temperatures were lower and CBL depths suppressed throughout the day.

Nonlocal changes included the collapse of the CBL after the passage of the LBF. In the 1992 run, the LBF was accelerated in the northern half of the SLV, but slowed in the southern half of the SLV relative to the 1847 run. This presents an interesting concern as future development (and development that has occurred since 1992) displaces agricultural land throughout the Wasatch Front area. This type of land cover replacement in the southern SLV could result in an acceleration of the LBF all the way to the Traverse Range. This would result in earlier decreases in CBL depths in the northern SLV.

REFERENCES

Atkinson, B. W., 2003: Numerical modeling of urban heat-island intensity. *Bound.-Layer Meteor.*, **109,** 285-310.

Black, T. L., 1994: The new NMC Mesoscale Eta Model: Description and forecast examples. *Wea. Forecasting*, **9,** 265-278.

Baidya Roy, S., C. P. Weaver, D. S. Nolan, and R. Avissar, 2003: A preferred scale for landscape forced mesoscale circulations? *J. Geophys. Res.*, **108** (D22), 8854, doi:10.1029/2002JD003097.

Bornstein, R. D., 1968: Observations of the urban heat island effect in New York City. *J. Appl. Meteor.*, **7,** 575-582.

Burian, S. J., S. P. Velugubantla, and M. J. Brown, 2002: Morphological analyses using 3-D building databases: Salt Lake City, UT. LA-UR-03-6197, Los Alamos National Laboratory.

Chase, T. N., R. A. Pielke, T. G. F. Kittel, J. S. Baron, and T. J. Stohlgren, 1999: Potential impacts on Colorado Rocky Mountain weather due to land use changes on the adjacent Great Plains. *J. Geophys. Res.*, **104,** 16,673-16,690.

Cottam, W. P. 1947: Is Utah Sahara bound? *University of Utah Bulletin*, **37,** 40

Defant, F., 1949: Zur theorie der hangwinde, nebst bemerkungen zur theorie der berg- und talwinde. [A theory of slope winds, along with remarks on the theory of mountain winds and valley winds]. Arch. Meteor. Geophys. Bioklim., A1, 421-450. (English translation: C. D. Whiteman, and E. Dreiseitl, 1984: Alpine meteorology: Translations of classic contributions by A. Wagner, E. Ekhart and F. Defant. Pacific Northwest Laboratory, Richland, Washington, 121 pp. [PNL-5141/ASCOT-84-3]).

de Wekker, S. F. J., 2002: Structure and morphology of the convective boundary layer in mountainous terrain. Ph.D. dissertation, University of British Columbia, 191 pp.

Diem, J. E., and D. P. Brown, 2002: Anthropogenic impacts on summer precipitation in central Arizona, U. S. A. *The Professional Geographer*, **55,** 343-355.

Doran, J. C., W. J. Shaw, and J. M. Hubbe, 1995: Boundary layer characteristics over areas of inhomogeneous surface fluxes. *J. Appl. Meteor.*, **34,** 559-571.

Doran, J. C., J. D. Fast, and J. Horel, 2002: The VTMX 2000 campaign. *Bull. Amer. Meteor. Soc.*, **83,** 537-551.

Draxler, R. R., 1986: Simulated and observed influence of the nocturnal urban heat island on the local wind field. *J. Clim. Appl. Meteor.*, **25,** 1125-1133.

Dudhia, J., 1989: Numerical study of convection observed during the Winter Monsoon Experiment using a mesoscale two-dimensional model. *J. Atmos. Sci.*, **46,** 3077-3107.

Grell, G. A., J. Dudhia, and D. R. Stauffer, 1995: A description of the fifth-generation Penn State/NCAR Mesoscale Model (MM5). NCAR Tech. Note NCAR/TN-398 + STR, 122 pp. [Available from UCAR Communications, P.O. Box 3000, Boulder, CO 80307.]

Grimmond, C. S. B., and T. R. Oke, 1995: Comparison of heat fluxes from summer-time observations in the suburbs of four North American cities. *J. Appl. Meteor.*, **34,** 873-889.

____ and ____, 1999: Aerodynamic properties of urban areas derived from analysis of surface form. *J. Appl. Meteor.*, **38,** 1262-1292.

Hanna, S. F., and R. Yang, 2001: Evaluations of mesoscale models' simulations of near-surface winds, temperature gradients, and mixing depths. *J. Appl. Meteor.*, **40,** 1095-1104.

Hart, K. A., W. J. Steenburgh, D. J. Onton and A. J. Siffert, 2004: An evaluation of mesoscale-model-based Model Output Statistics (MOS) during the 2002 Olympic and Paralympic Winter Games. *Wea. Forecasting*, **19,** 200-218.

Hawkes, H. B., 1947: Mountain and valley winds with special reference to the diurnal mountain winds of the Great Salt Lake region. Ph.D. dissertation, Ohio State University, 312 pp.

Henderson-Sellers, A., A. J. Pitman, P. K. Love, P. Irannejad, and T. H. Chen, 1995: The project for intercomparison of land surface parameterization schemes (PILPS): Phases 2 and 3. *Bull. Amer. Meteor. Soc.*, **76,** 489-503.

Hertig, J.-A., 1995: The heat island of the urban boundary layer: characteristics, causes, and effects. *Wind Climate in Cities*, J. E. Cermak et al., Eds., Kluwer Academic, 353-382.

Hong, S.-Y., and H.-L. Pan, 1996: Nonlocal boundary layer vertical diffusion in a medium-range forecast model. *Mon. Wea. Rev.*, **124,** 2322-2339.

Horel, J., and coauthors, 2002: Mesowest: Cooperative mesonets in the western United States. *Bull. Amer. Meteor. Soc.*, **83,** 211-225.

Howard, L., 1833: *The Climate of London*, Vols. I-III, London.

Huff, F. A., and S. A. Changnon, 1973: Precipitation modification by major urban areas. *Bull. Amer. Meteor. Soc.*, **54,** 1220-1232.

Ivans, Sasha, 2005: Response of water vapor and CO2 fluxes in semi-arid plant communities. Ph.D. dissertation, Utah State University, 119 pp.

Kain, J. S., 2004: The Kain-Fritsch convective parameterization: An update. *J. Appl. Meteor.*, **43,** 170-181.

Kitada, T., K. Okamura, and S. Tanaka, 1998: Effects of topography and urbanization on local winds and thermal environment in the Nohbi Plain, coastal region of central Japan: A numerical analysis by mesoscale meteorological model with a k-ε turbulence model. *J. Appl. Meteor.*, **37,** 1026-1046.

Kuwagata, T., and F. Kimura, 1995: Daytime boundary layer evolution in a deep valley. Part I: Observations in the Ina Valley. *J. Appl. Meteor.*, **34,** 1082-1091.

Kuwagata, T., and F. Kimura, 1997: Daytime boundary layer evolution in a deep valley. Part II: Numerical simulation of the cross-valley circulation. *J. Appl. Meteor.*, **36,** 883-895.

Lakhtakia, M. N., and T. T. Warner, 1994: A comparison of simple and complex treatments of surface hydrology and thermodynamics suitable for mesoscale atmospheric models. *Mon. Wea. Rev.*, **122,** 880-896.

Mahrer, Y., and R. A. Pielke, 1977: The effects of topography on sea and land breezes in a two-dimensional numerical model. *Mon. Wea. Rev.*, **105,** 1151-1162.

Mahrt, L., 1982: Momentum balance of gravity flows. *J. Atmos. Sci.*, **39,** 2701-2711.

Malek, E., and G. E. Bingham, 1997: Partitioning of radiation and energy balance components in an inhomogeneous desert valley. *J. Arid Environ.*, **37,** 193-207.

Marshall, C., R. A. Pielke, L. T. Steyaert, and D. A. Willard, 2004: The impact of anthropogenic land-cover change on the Florida peninsula sea-breezes and warm season sensible weather. *Mon. Wea. Rev.*, **132,** 28-52.

McNider, R. T., and R. A. Pielke, 1984: Numerical simulation of slope and mountain flows. *J. Clim. Appl. Meteor.*, **23,** 1441-1453.

Morris, C. J. G., I. Simmonds, and N. Plummer, 2001: Quantification of the influences of wind and cloud on the nocturnal urban heat island of a large city. *J. Appl. Meteor.*, **40,** 169-182.

Neumann, J., 1973: The sea and land breezes in the classical Greek literature. *Bull. Amer. Meteor. Soc.*, **54,** 5-8.

Ohashi, Y., and H. Kida, 2002: Local circulations developed in the vicinity of both coastal and inland urban areas: a numerical study with a mesoscale atmospheric model. *J. Appl. Meteor.*, **41,** 30-45.

Oke, T. R., 1982: The energetic basis of the urban heat island. *Quart. J. Roy. Meteor. Soc.*, **108,** 1-24.

Oke, T. R., 1995: The heat island of the urban boundary layer: characteristics, causes, and effects. *Wind Climate in Cities*, J. E. Cermak et al., Eds., Kluwer Academic, 81-107.

Pielke, R. A., J. H. Rodriguez, J. L. Eastman, R. L. Walko, and R. A. Stocker, 1993: Influence of albedo variability in complex terrain on mesoscale systems. *J. Climate*, **6,** 1798-1806.

Pielke, R. A., R. L. Walko, L. T. Steyaert, P. L. Vidale, G. E. Liston, W. A. Lyons, and T. N. Chase, 1999: The influence of anthropogenic landscape changes on weather in South Florida. *Mon. Wea. Rev.*, **127,** 1663-1673.

Poulos, G. S., 1996: The interaction of katabatic winds and mountain waves. Ph.D. dissertation, Colorado State University, 399 pp. [Available from Colorado State University, Dept. of Atmospheric Sciences, Fort Collins, CO 80523.]

Prandtl, L., 1952: *Essentials of Fluid Dynamics*. Hafner, 452 pp.

Rampanelli, G., D. Zardi, and R. Rotunno, 2004: Mechanisms of up-valley winds. *J. Atmos. Sci.*, **61,** 3097-3111.

Reible, D. D., J. E. Simpson, and P. F. Linden, 1993: The sea breeze and gravity-current frontogenesis. *Quart. J. Roy. Meteor. Soc.*, **119,** 1-16.

Reuten, C., D. G. Steyn, K. B. Strawbridge, and P. Bovis, 2005: Observations of the relation between upslope flows and the convective boundary layer in steep terrain. *Bound.-Layer Meteor.*, **116,** 37-61.

Rife, D. L., T. T. Warner, F. Chen, and E. G. Astling, 2002: Mechanisms for diurnal boundary layer circulations in the Great Basin Desert. *Mon. Wea. Rev.*, **130,** 921-938.

Rogers, E., T. Black, D. Deaven, G. DiMego, Q. Zhao, Y. Lin, N. W. Junker, and M. Baldwin, 1995: Changes to the NMC operational Eta model analysis/forecast system. NWS Tech. Procedures Bull. 423, 51 pp. [Available from National Weather Service, Office of Meteorology, 1325 East-West Highway, Silver Springs, MD 20910.]

Rogers, E. T., T. Black, D. Deaven, G. DiMego, Q. Zhao, M. Baldwin, and N. M. Junker, 1996: Changes to the operational "early" Eta analysis/forecast system at the National Centers for Environmental Prediction. *Wea. Forecasting*, **11,** 391-413.

Rotunno, R., 1983: On the linear theory of the land and sea breeze. *J. Atmos. Sci.*, **40,** 1999-2009.

Ruddiman, W. F., 2003: The anthropogenic greenhouse era began thousands of years ago. *Clim. Change*, **61,** 261-293.

Sailor, D. J., 1995: Simulated urban climate response to modifications in surface albedo and vegetative cover. *J. Appl. Meteor.*, **34,** 1694-1704.

Schultz, P., and T. T. Warner, 1982: Characteristics of summertime circulations and pollution ventilation in the Los Angeles Basin. *J. Appl. Meteor.*, **21,** 672-682.

Segal, M., and R. W. Arritt, 1992: Nonclassical mesoscale circulations caused by surface sensible heat-flux gradients. *Bull. Amer. Meteor. Soc.*, **73,** 1593-1604.

Segal, M., J. R. Garratt, R. A. Pielke, W. E. Schreiber, A. Rodi, G. Kallos, and J. Weaver, 1989: The impact of crop areas in northeast Colorado on midsummer mesoscale thermal circulations. *Mon. Wea. Rev.*, **117,** 809-825.

Segal, M., J. H. Cramer, R. A. Pielke, J. R. Garratt, and P. Hildebrand, 1991: Observational evaluation of the snow breeze. *Mon. Wea. Rev.*, **119,** 412-424.

Segal, M., M. Leuthold, R. W. Arritt, C. Anderson, and J. Shen, 1997: Small lake daytime breezes: some observational and conceptual evaluations. *Bull. Amer. Meteor. Soc.*, **78,** 1135-1147.

Sellers, P. J., Y. Mintz, Y. C. Sud, and A. Dalcher, 1986: A simple biosphere model (SiB) for use within general circulation models. *J. Atmos. Sci.*, **43,** 505-631.

Shaw, W. J., and J. M. Hubbe, 2002: Structure of the atmospheric boundary layer in the central Salt Lake Valley during the afternoon-to-evening transition. Preprints, *10th Conf. on Mountain Meteorology*, Park City, UT, Amer. Meteor. Soc., 112-115.

Shepherd, J. M., and S. J. Burian, 2003: Detection of urban-induced rainfall anomalies in a major coastal city. Earth Interactions, **7**. [Available online at http://EarthInteractions.org.]

Simpson, J. E., 1994: *Sea breeze and local winds*. Cambridge University Press, 234 pp.

Souza, E. P., N. O. Rennó, M. A. F. Silva Davis, 2000: Convective circulations induced by surface heterogeneities. *J. Atmos. Sci.*, **57,** 2915-2922.

Steenburgh, W. J., S. F. Halvorson, and D. J. Onton, 2000: Climatology of lake-effect snowstorms of the Great Salt Lake. *Mon. Wea. Rev.*, **128,** 709-727.

Stewart, G., 1941: Historic records bearing on agricultural and grazing ecology in Utah. *J. Forestry*, **39,** 362-375.

Stewart, J. Q., C. D. Whiteman, W. J. Steenburgh, and X. Bian, 2002: A climatological study of thermally driven wind systems of the U. S. Intermountain West. *Bull. Amer. Meteor. Soc.*, **83,** 699-708.

Stivari, S. M., A. P. de Oliveira, H. A. Karam, and J. Soares, 2003: Patterns of local circulation in the Itaipu Lake area: Numerical simulations of lake breeze. *J. Appl. Meteor.*, **42,** 37-50.

Stone, G. L., and D. E. Hoard, 1990: Daytime wind in valleys adjacent to the Great Salt Lake. Preprints, Fifth Conference on Mountain Meteorology, June 25-29, 1990, Boulder, CO.

Stull, R. B., 1988: *An Introduction to Boundary Layer Meteorology*. Kluwer Academic Publishers, 666 pp.

Troen, I., and L. Mahrt, 1986: A simple model of the atmospheric boundary layer; Sensitivity to surface evaporation. *Bound.- Layer Meteor.*, **37,** 129-148.

United Nations, 2004: *World urbanization prospects: the 2003 revision*. United Nations, 335 pp.

Vogelmann, J. E., S. M. Howard, L. Yang, C. R. Larson, B. K. Wylie, N. Van Driel, 2001: Completion of the 1990s National Land Cover Data Set for the conterminous United States from Landsat Thematic Mapper data and ancillary data sources. *Photogrammetric Engineering and Remote Sensing*, **67,** 650-652.

Walko, R. L, and coauthors, 2000: Coupled atmosphere-biophysics-hydrology models for environmental modeling. *J. Appl. Meteor.*, **39,** 931-944.

Weigel, A. P., 2005: On the atmospheric boundary layer over highly complex topography. Ph.D. dissertation, Swiss Federal Institute of Technology, 153 pp.

Whiteman, C. D., 1982: Breakup of temperature inversions in deep mountain valleys: Part I. Observations. *J. Appl. Meteor.*, **21,** 270-289.

Whiteman, C. D., 1990: Observations of thermally developed wind systems in mountainous terrain. *Atmospheric Processes over Complex Terrain, Meteor. Monogr.*, No. 45, Amer. Meteor. Soc., 5-42.

Yoshikado, H., 1992: Numerical study of the daytime urban effect and its interaction with the sea breeze. *J. Appl. Meteor.*, **31,** 1146-1164.

Yoshikado, H., and M. Tsuchida, 1996: High levels of winter air pollution under the influence of the urban heat island along the shore of Tokyo Bay. *J. Appl. Meteor.*, **35,** 1804-1813.

Zeller, K. F., 1972: The mountain and thermal effects on the planetary boundary layer in the Salt Lake Valley. M.S. thesis, University of Utah, 93 pp.

Zhong, S., and J. C. Doran, 1995: A modeling study of the effects of inhomogeneous surface fluxes on boundary-layer properties. *J. Atmos. Sci.*, **52,** 3129-3142.

Zhong, S., and J. Fast, 2003: An evaluation of the MM5, RAMS, and Meso-Eta models at subkilometer resolution using VTMX field campaign data in the Salt Lake Valley. *Mon. Wea. Rev.*, **131,** 1301-1322.

Zumpfe, D., 2004: A case study of a strong lake-breeze front in the Salt Lake Valley. M.S. thesis, University of Utah, 72 pp.